Journal of Cleaner Production 332 (2022) 130039

Contents lists available at ScienceDirect

Journal of Cleaner Production

journal homepage: www.elsevier.com/locate/jclepro

Sustainable toxic dyes removal with advanced materials for clean water production: A comprehensive review

Siow Hwa Teo [a,b,1], Chi Huey Ng [c,1,*], Aminul Islam [d,e,1,**], G. Abdulkareem-Alsultan [b], Collin G. Joseph [a], Jidon Janaun [c], Yun Hin Taufiq-Yap [a,b], Shahjalal Khandaker [f], Gazi Jahirul Islam [g], Hussein Znad [h,j], Md. Rabiul Awual [h,i,***]

[a] Industrial Chemistry Program, Faculty Science and Natural Resources, Universiti Malaysia Sabah, 88400, Kota Kinabalu, Sabah, Malaysia
[b] Catalysis Science and Technology Research Centre, Faculty of Science, Universiti Putra Malaysia, 43400, Serdang, Selangor, Malaysia
[c] Chemical Engineering Programe, Faculty of Engineering, Universiti Malaysia Sabah, 88400, Kota Kinabalu, Sabah, Malaysia
[d] Department of Petroleum and Mining Engineering, Jashore University of Science and Technology, Jashore, 7408, Bangladesh
[e] Clean Energy and CO_2 Capture Lab, Jashore University of Science and Technology, Jashore, 10 7408, Bangladesh
[f] Department of Textile Engineering, Dhaka University of Engineering & Technology, Gazipur, 1707, Bangladesh
[g] Department of Chemistry, University of Barisal, Bangladesh
[h] Western Australian School of Mines: Minerals, Energy and Chemical Engineering, Curtin University, GPO Box U 1987, Perth, WA, 6845, Australia
[i] Materials Science and Research Center, Japan Atomic Energy Agency (JAEA), Hyogo, 679-5148, Japan
[j] School of Engineering, Edith Cowan University (ECU), Perth, WA, 6027, Australia

ARTICLE INFO

Handling Editor: Prof. Jiri Jaromir Klemeš

Keywords:
Toxic dyes
Composite materials
Degradation
Adsorbents
Sustainability
Clean water production

ABSTRACT

Textile dye is one of the significant pollutants of water worldwide. However, dumping the textile effluent to the environment is a common in most of the developing countries. Contaminated water in the textile industry may contain various toxic ingredients and people were easily infected with various diseases. The contamination may affect the marine environment and consequently extends around the world. The recycling of waste water is the significant option to reduce the environmental pollution. In particular, adsorption approach is one of the significant strategies to treat dye-contaminated water due to their advantageous of physico-chemical properties. In this review paper, variety of potential adsorbents for dye removal were critically reviewed, focusing on the efficient adsorbent to remediate dye-contaminated water. Specifically, the recent development of adsorbents containing carbon, metal supported adsorbents, surface functionalized gel adsorbents and photo-adsorbents were reviewed focusing on cutting-edge processes. Comparison of degradation efficiency for different adsorbents, synthesis approaches and their physico-chemical properties were assessed in systematic way. The perspective of the adsorbent materials associated with the dye degradation was discussed thoroughly. The evaluation of different advanced materials would contribute to the development of the sustainable dye removal process in near future.

1. Introduction

Dyeing the fabric is one of the most polluter of water and textile dyeing is the second-largest polluter of water worldwide (Okafor et al., 2021). According to a United Nations World Water Development report, more than 80% of all the wastewater from different sectors is released to the environment without adequate treatment (Kataki et al., 2021). Releasing the fashion pollution from textile dyeing contaminates the groundwater. The repeated throwing of waste water into the environment reduces the necessary nutrients and fertilities from the soil. According to UNICEF, millions of people die each year due to the drinking of contaminated water (UNICEF, 2019). General public and policy maker should have strong commitment to manage waste water in a sustainable way. Hence, wastewater treatment is a significant issue that

* Corresponding author. Chemical Engineering Programe, Faculty of Engineering, Universiti Malaysia Sabah, 88400 Kota Kinabalu, Sabah, Malaysia.
** Corresponding author. Department of Petroleum and Mining Engineering, Jashore University of Science and Technology, Jashore, 7408, Bangladesh.
*** Corresponding author. Materials Science and Research Center, Japan Atomic Energy Agency (JAEA), Hyogo 679-5148, Japan.
E-mail addresses: chihueyng@ums.edu.my (C.H. Ng), aminul_pme@just.edu.bd (A. Islam), rawual76@yahoo.com (Md.R. Awual).
[1] These authors were contributed equally.

https://doi.org/10.1016/j.jclepro.2021.130039
Received 8 June 2021; Received in revised form 4 December 2021; Accepted 7 December 2021
Available online 11 December 2021

has been addressed by several researchers to find a sustainable treatment approach (Ibrahim et al., 2021a,b; Khandaker et al., 2021; Roy et al., 2022; Miah et al., 2021; Swaraz et al., 2021).

Several studies have been concentrated to develop efficient adsorbent for wastewater treatment (Najafi et al., 2021; Qi et al., 2021; Kubra et al., 2021a,b; Khan et al., 2021a,b; Salman et al., 2021). Carbon and their composite materials was reported promising adsorbent for the removal of different types of dyes (Khan et al., 2021a,b; Ibrahim et al., 2021a,b; Hasan et al., 2021, 2021a; Chowdhury et al., 2021; Rahman et al., 2020). The wide spectrum of waste water treatment using advanced carbon materials with engineered design was reported in the literature (Singh et al., 2021; Sultana et al., 2020). The ensnarement of various active materials with carbon-based composites showed noteworthy benefits because of their high surface area, tunable morphology (Dong et al., 2021). It is reasonable to mention that the complex synthesis process of adsorbent may not viable for industrial application.

Many researchers have focused on the application of the hydrogels and photocatalyst for the removal of dyes and various pollutants over the past few decades (Akter et al., 2021; Pereira et al., 2021; SinarMashuri et al., 2020; Taufiq-Yap et al., 2021; Hayase, 2021). The hydrogels prepared from the polymers are shown efficient for the removal of different kinds of pollutants (Akter et al., 2021). The use of semiconductor photocatalyst has been focused for the removal of pollutants from aqueous solution (Nasir et al., 2021; Suresh et al., 2021; Teo et al., 2021; Mansir et al., 2019; Taufiq-Yap et al., 2019). The narrower bandgap, tunable morphology, reduced electron/hole recombination properties are the main strength of photocatalyst for efficiently removal of contamination from water (Ray et al., 2021; Ghosh et al., 2018; How et al., 2017).

The use of electrocoagulation (EC) is a promising method for treating wastewater and removing dyes, due to the due to its simple operation, high removal efficiency, and reduced sludge production (Asfaha et al., 2021; Jing et al., 2021). Therefore, many researchers have concentrated to using electrocoagulation for wastewater treatment. Typically, the electrocoagulation/flocculation process, using composite materials such as aluminium and Iron could increase the environmental pollution levels by introducing non-biodegradable compounds (Igwegbe et al., 2021). The effectiveness of the EC process depends on the electrolyte concentration, pH, current density, applied voltage, operating temperature, electrode material and configurations. These variables would affect the overall removal efficiency, reaction kinetics, and treatment time (Igwegbe et al., 2021). Given the substantial number of studies on electrocoagulation, a conclusion has been reached by several researchers that EC process is efficient for the laboratory-scale tests.

Some emerging novel carbon composite for efficient removal of pollutants has been discussed by several researchers (Dong et al., 2021; Nasrollahzadeh et al., 2021; Janaun et al., 2016). Overall, these articles focused on composition of vcarbon providing limited view regarding to a broad research field. The sustainable bio-adsorbents for waste water treatment were reviewed by several researchers (Sheth et al., 2021; Solangi et al., 2021; Shahat et al., 2021) and effect of various operating parameters and future scope of the bioadsorbent were focused. Reviews on novel metal compoaiteadsorbent for heavy metal adsorption from wastewater have been published (Chai et al., 2021). Some attentions have been paid on the sustainability of dye removal from waste water-using graphene based materials, especially, broad discussion on the graphene-based hybrid membrane materials were reported (Bhol et al., 2021; Velusamy et al., 2021). Works on the dye removal by photocatalyst and its detail properties have been reported aiming to find the efficient photocatalyst catalyst for waste water treatment (Nasir et al., 2021). An alternative approach to degradate from waste water using metal-organic framework (MOFs) membranes focusing the multifactors influenced on the MOF membranes (Uddin et al., 2021; Yu et al., 2021). However, only a limited review has been focused on the comprehensive catalytic adsorption process for dye degradation from waste water.

An attempt has been made in this review to provide overall catalytic adsorption process for dye degradation aiming to find the most efficient adsorption process. A critical discussion on the adsorbent properties and their mechanism involved in the dye degradation process has been provided. A comparison of several group of adsorbents and the future perspective towards the dye degradation has been outlined. This study will be useful to select suitable adsorbent in various dye degradation process and improve the knowledge about the cutting-edged adsorbent.

2. Basic principles of dyes adsorption

Adsorption emerges as an appealing technique to eliminate organic and natural pollutants such as dyes from the environment because the disposal of dyes such as azo, anthraquinone, nitrio, etc. into the water bodies may plunge the penetration of sunlight, consequently affect the marine life and environment (Javaid and Qazi, 2019). Adsorption is classified as a surface phenomenon, particularly, the adsorbate (molecule or ion) is adsorbed on the surface of adsorbent without penetrating into the adsorbent structure (Han et al., 2021) as shown in Fig. 1. Adsorption is basically happened in a physical or chemical way when the surface particles of the adsorbent (also known as surface energy) exhibiting irregular or leftover attractive forces that are inequivalent with the particles of bulk adsorbent. In this regard, having all the forces which are stabilized together and the excessive forces would attract adsorbate to the surface of adsorbent (Hessou et al., 2019; Alam et al., 2019; Abbas et al., 2018). Physical adsorption is the interaction between the adsorbent and adsorbate surface via weak van der Waals force where the weak bonding between adsorbate-adsorbent results in a reversible adsorption and desorption processes. Meanwhile, chemisorption is an irreversible process where adsorbate adsorbed to the surface of functional adsorbent through strong covalent bonds or electrostatic attraction, achieving effective separation (Zhou et al., 2019; Abdulkareem-Alsultan et al., 2022; Asikin-Mijan et al., 2021). Mutalib et al. (2020). Chemisorption is usually the monolayer generated on the adsorbent surface and happened at extremely high temperature than the critical temperature. Whilst, physisorption is usually multilayer generated on the adsorbent surface (Xia et al., 2019; Lee et al., 2019; Zainal et al., 2019; Ng et al., 2018). Three main steps to kick start the adsorption process includes (i) transport of dyes molecules to the absorbent's surface from an aqueous solution, (ii) adsorption of them onto the sorbent surface, and (iii) transport within the sorbent particle (Chai et al., 2021; Angove et al., 2019).

An effective adsorbent material should possess excellent mechanical properties, high surface area, and adequate functional groups such as hydroxyl, amine, etc., suitable pore size (Zhu et al., 2019; Rachel-Tang et al., 2017; Chan et al., 2012; Mansa et al., 2012; Bakar et al., 2013). Additionally, the structure and crystal orientation of the adsorbent are also the important factors determine the efficiencies of adsorption. There are a variety of natural or synthetic adsorbents existing in different nature which can be readily used in its original form or modified version for dye removal from wastewater such as the carbonaceous, gel, metal, and photocatalyst-based sorbents, which will be discussed in the following section.

2.1. Carbon-based adsorbents

Carbonaceous materials are profound in contaminants removal in wastewater ascribed to its abundant pores and available functional groups such as phenol, carboxyl, carbonyl, etc., which would bind to the dye molecules or complexes chemically or physically, subsequently removing them (dyes) from the aqueous solution. Among the carbonaceous materials, activated carbon (AC) is of widely use owing to its microporous structure, large surface area and chemical complexity properties, as well as its simplicity of design and high reusability. This carbon-based material could be manufactured from pyrolysis and activation of wood, coal, lignite, and other high carbon-containing raw materials, thereby could be moulded into amorphous carbon solid of

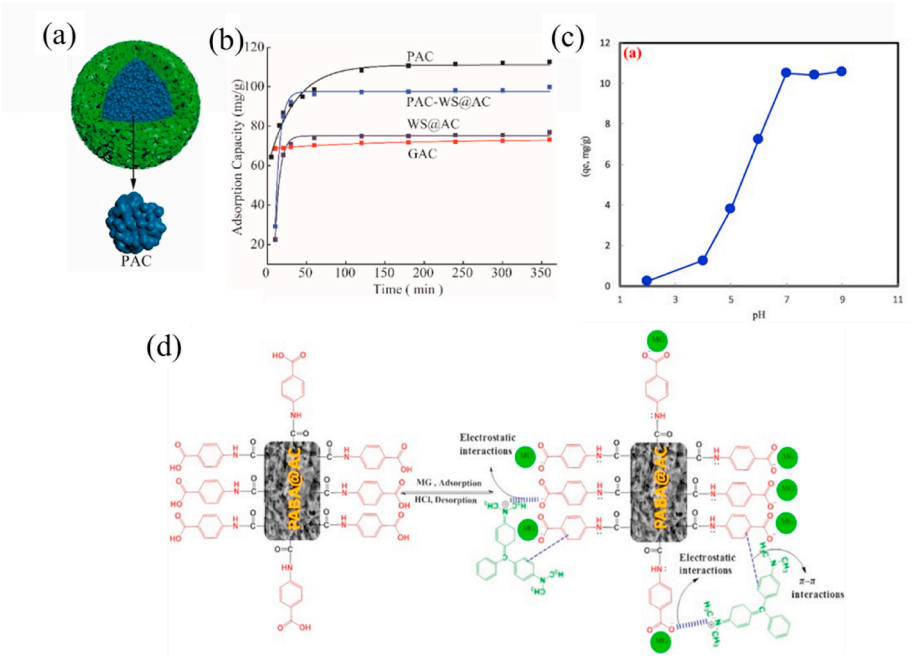

Fig. 1. (a) The diagrammatic drawing of WS@AC, (b) effect of contact time on the removal of trypan blue by PAC, GAC, WS@AC, and PAC-WS@AC (Z. Cai et al., 2020b), (c) effect of pH on PABA@AC composite, and (d) mechanism for the adsorption/desorption of MG dye onto PABA@AC composite (Naushad et al., 2019).

various shapes such as powder, granular, fibrous, and honeycomb (Ahmad and Azam, 2019; Chai et al., 2021; Chengyu Duan et al., 2020a, b). The adsorption capacity of AC can be increased by physical and chemical treatment, whereby physical activation is usually achieved through carbonization with steam where the product is pyrolyzed to extract non-carbon components, followed by gases-assisted activation process at temperature of 700–1100 °C to improve the porous structure of the carbonized material. Chemical activation, on the other hand, is a one-step process used to prepare AC using various chemical activating substances (Rathi and Kumar, 2021). Since AC derived from coal is expensive, it has thus prompted for the exploration of low-cost raw materials, developed from abundant and various agricultural waste materials. For instance,a cost-effective powdered activated carbon (PAC) was synthesized from rubber sees (RS) and RSS (rubber seed shells (RSS) for methylene blue dye removal from aqueous solution using carbonization, KOH, NaOH, and H_2SO_4 activation. Results show that PAC impregnated with NaOH (RSS) and H_2SO_4 (RS) showed the best adsorption capability, credited to the pore size structure of NaOH, as well as the available functional groups include -OH, -NH, C=C, C=N, and C=O, as evidence of the formation of hydrogen bonding between the functional groups (Nizam et al., 2021).

Nevertheless, one issue of PAC is that it cause secondary pollution because of the difficulties in separating thePAC from the medium. Alternatively, ACs in the form of granular (GAC)is introduced. GAC is freed from both aforementioned issues (dust pollution and separation), however, the use of binder during the synthesis process may cause undesirable blockage over the pores structure of the sorbent and thus reduces the adsorption capacity of GAC. As a solution to the binder issue, Cai et al. (2020a,b) has successfully designed a novel binderlesscore-shell granular AC, denoted as WS@AC.The core of the catalyst is composed of PAC, while silica sol and wood powder formed the shell (Fig. 1a). The novelty of this work is that the PAC core was formed without the need of a binder, making PAC achieving the highest adsorption capacity of 113.2 mg/g (Fig. 1b), which is far higher than the work reported in literature (48.54 mg/g by functionalized graphene oxide-based hydrogels). This phenomenon could be ascribed to the high specific surface area of 1127.8 m^2/g achieved by WS@AC, additioning to the 3D open pore network structure of the GAC shell that enhances the entering and adsorption of adsorbates to the PAC core (Cai et al., 2020a, b). In another work reported by Naushad and co-workers, they functionalized AC with P-aminobenzoic acid (PABA) to remove malachite green (MG) dye from aqueous solution (Naushad et al., 2019). They demonstrated that pH is an important factor affects the adsorption capacity by the degree of ionization of adsorbent surface. Fig. 1c shows that the adsorption capacity of MG improved from a pH of 2.0–7.0 owing to the reduction of the density of positive charge on the surface sites of PABA@AC composite, thereby improved the adsorption efficiency of PABA@AC via electrostatic and π-π interactions (Fig. 1d). An acidic medium lead to inferior adsorption ability due to the competition between hydronium ions and MG cations for the active sites on the catalyst surface. Meanwhile, a basic medium alters the structure of MG molecules and consequently plunges the adsorption capacity (Bhagavathi Pushpa et al., 2015).

In general, the activation treatment of AC usually leads to microporous features on the carbon surface, which generally results in relatively lower absorption capacity attributed to the size exclusion effect (Liu et al., 2016). Graphene and its derivatives are the next rising stars for organic pollutants and dyes removal from the industrial effluents owing to its high theoretical surface area (2630 m^2/g) of a single graphene (Ng et al., 2017). The removal efficiency of graphene-based materials is monitored by their interaction with the dye molecules, surface area, porosity, nature of dyes, pH, etc. The presence of defect sites, oxygenated groups, wrinkles and π-electron domains in the planar structure of rGO promise the potential of reduced graphene oxide (rGO) as an excellent adsorbent because the presence of negatively charged oxygen functionalities (carboxylic, phenolic, hydroxyl, etc.) in the GO and its composites serve ample adsorption sites for the adsorption of cationic dyes. In 2017, Gupta and Khatri have proven the effectiveness of rGO in removing MG dye from simulated wastewater, in which the cationic dyes are well-adsorbed on the rGO (476.2 mg/g) than that of anionic dyes, typically faster at higher pH (75 min compared to lower pH at a slower rate of 420 min) (Gupta and Khatri, 2017), as depicted in Fig. 2a. This is because electrostatic attractive interaction between the negatively charged surface of rGO and MG cationic dye increases at a higher pH (neutral and alkaline pH), hence sped up the adsorption process (Erickson et al., 2010). Up to this point, it should be cleared that

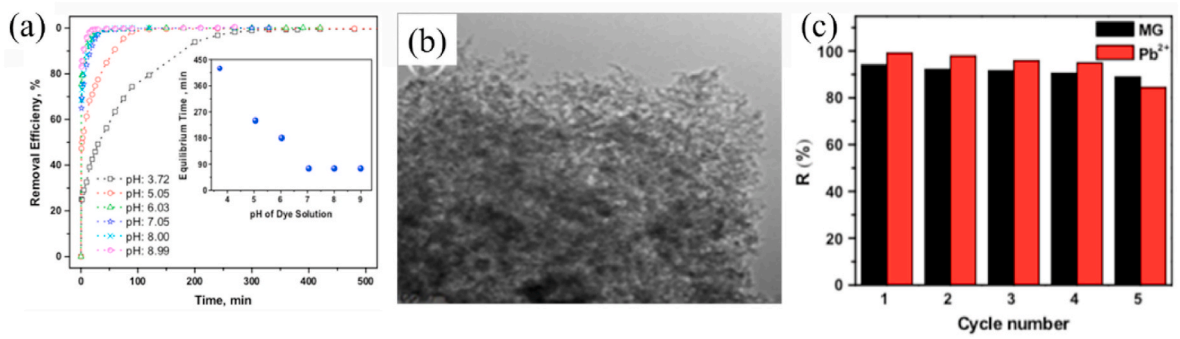

Fig. 2. (a) Effect of pH on removal of MG dye using the rGO as an adsorbent. Inset graph shows changes in equilibrium time as a function of pH, initial concentration of MG dye: 100 mg/L, (b) TEM image of OMC, and (c) recycle experiment for MG (m = 10 mg, C_o = 500 mg/L, V = 20 mL, pH = 6.5, temperature at 298 K) and Pb^{2+} (m = 10 mg, C_o = 100 mg/L, V = 20 mL, pH = 5, temperature at 303 K) (Gupta and Khatri, 2017).

the adsorption of dye molecules is greatly influenced by the pH because it alters the surface charge by changing the nature of the functional groups grafted on the adsorbent. In another work, Zhang et al., designed an oxidized mesoporous carbon (OMC) with fluffy structure from graphitic mesoporous carbon (GMC) followed by oxidation via a modified Hummers' method to remove MG dyes (Barton et al., 1984). Fig. 2b shows that the synthesized OMC has a fluffy ultrathin-wall structure with narrow pore size distribution and rich oxygen-containing groups. The in-situ formation of GO-like structure is not merely improving surface hydrophilicity of the OMC, but also providing abundant active istes for adsorption, thus lead to a maximum adsorption capacity of 963.1 mg/g that can be maintained after several regeneration cycles (Fig. 2c), implies OMC is a promising absorbent for dyes removal from wastewater (Ahmad et al., 2014; Zhang et al., 2018). As a summary, among the factors (pH, temperature, contact time, initial concentration), pH control is the most critical point to be carefully considered because at low pH, an inevitable competition between dyes and H^+ for active sites would be happened, while the change of surface charge is inevitably happened at high pH. The carbon-based absorbents are tabulated in Table 1.

Regeneration is an important context in the development of AC because it helps to restore the adsorption capacity of an exhausted adsorbent and for further reuse, thus making the technology cost effective (Awual, 2019, 2019a, 2019b, 2019c, 2019d, 2019e; 2019f) (see Table 2). The conventional recovery approach such as thermal regeneration method is time-consuming and costly in terms of energy consumption. Worstly, about 40% carbon was loss during the recovery step of powder-activated carbon, as reported in literature (Li et al., 2011; Lu et al., 2011; Moosavi et al., 2020; Shende and Mahajani, 2002). In regard to enhance the regeneration and reusability of the catalysts, magnetic separation using magnetic adsorbents arises as a promising way to recover adsorbents and control the adsorption process, hence increase the regeneration abilities of adsorbents (Awual, 2015, 2016, 2016a, 2016b, 2017, 2017a). For instance, magnetically functionalized multiwall carbon nanotube (MMWCNT) composed of commercial MWCNT and iron oxide nanoparticles was prepared to remove cationinc dyes from aqueous solution, however, this reported carbon material was unsatisfactory in keeping both high adsorption capacity and rapid magnetic separation due to nonspecific adsorption and slow mass transfer kinetics (Altintig et al., 2017, 2018, 2021; Gong et al., 2009; Zirak et al., 2018; Tuzen et al., 2018). In 2019, Li and co-workers studied the adsorption of malachite green (MG) from aqueous solution using a new type of adsorbent composed of magnetic graphene oxide decorated with persimmon tannins (Fe_3O_4/PT/GO) composites synthesized from one-spot hydrothermal method (Gao et al., 2019). Three independent variables, including pH, Fe_3O_4/PT/GO dosage, and initial MG concentration. The Fe_3O_4/PT/GO composite demonstrated outstanding adsorption ability with the extremelly high adsorption capacity of

Table 1
Carbon based adsorbent with different surface functionalizations.

Catalyst	Parameters	Pollutant	Efficiency (mg/g)	Ref.
Sulfonic acid modified powder activated carbon (H_2SO_4-PAC)	pH 4; T = 25 °C; time t = 25min	Methylene blue (MB)	769	Nizam et al. (2021)
Sodium hydroxide modified powder activated carbon (NaOH-PAC)	pH 4; T = 25 °C; time t = 25min	Congo red (CR)	458	Nizam et al. (2021)
Wood powder and silica sol modified core-shell granular activated carbon (WS@AC)	pH 2; T = 25 °C; time t = 50min	Trypan blue (TB)	113	(Z. Cai et al., 2020b)
P-aminobenzoic acid functionalized activated carbon (PABA@AC)	pH 7; T = 25 °C; time t = 240min	Malachite green (MG)	67	Naushad et al. (2019)
Effective microorganism activated kitchen solid waste carbon	pH 8; T = 30 °C; time t = 100min	Malachite green (MG)	159	Bhagavathi Pushpa et al. (2015)
Reduced graphene oxide	pH 3.7; T = 25 °C; time t = 420min	Malachite green (MG)	476	Gupta and Khatri (2017)
KOH treated durian seed-based activated carbon (DSAC)	pH 8; T = 60 °C; time t above 1320min	Malachite green (MG)	371	Ahmad et al. (2014)
Oxidized mesoporous carbon (OMC)	pH 6.5; T = 40 °C; time t above 360min	Malachite green (MG)	963	Zhang et al. (2018)
Polyethylenimine functionalized coffee waste derived carbon (PEI-CW)	pH 3; T = 25 °C; time t above 50min	Reactive Black 5 (RB5)	78	Wong et al. (2020)
Polyethylenimine functionalized coffee waste derived carbon (PEI-CW)	pH 3; T = 25 °C; time t above 106min	Congo Red	34	Wong et al. (2020)
H2SO4 activated *Annona squmosa* seed carbon	pH 6; T = 27 °C; time t above 100min	Malachite green (MG)	26	Santhi et al. (2016)
H2SO4 activated *Annona squmosa* seed carbon	pH 6; T = 27 °C; time t above 100min	Methylene blue (MB)	9	Santhi et al. (2016)

Table 2
Different modified carbon for dye removal.

Catalyst	Surface area (m2/g)	Pollutant	Loading (catalyst/ [a]pollutant)	Reaction conditions			Efficiency (%)	Regeneration (cycles)	Ref.
				T (^oC)	pH	T (min)			
Fe_3O_4 or γ-Fe_2O_3 coated multi-wall carbon nanotube (MMWCNT)	61.74	Methylene blue (MB)	0.5 g/3.74 mg/L	25	<7	360	[b]15.87 mg/g	−/−	Gong et al. (2009)
Fe_3O_4 or γ-Fe_2O_3 coated multi-wall carbon nanotube (MMWCNT)	61.74	Neutral red (NR)	0.5 g/2.89 mg/L	25	<7	360	20.51 mg/g	−/−	Gong et al. (2009)
Fe_3O_4 or Fe_2O_3 coated multi-wall carbon nanotube (MMWCNT)	61.74	Brilliant cresyl blue (BCB)	0.5 g/3.18 mg/L	25	<7	360	23 mg/g	−/−	Gong et al. (2009)
Fe3O4/PT/GO	53.83	Malachite green (MG)	0.015 g/150 mg/L	35	6	250	561 mg/g	5/85	Gao et al. (2019)
Magnetic (γ-Fe_2O_3) sugarcane bagasse activated carbon (MSBAC)	109.07	Methylene blue (MB)	5 g/50–400 mg/L	30	2–10	120	36 mg/g	4/>83	Jiang et al. (2021)
Fe_3O_4 magnetic nanoparticles functionalized activated carbon (Fe_3O_4/AC)	1200	Rhodamine B (RhB)	0.02 g/250 mg/L	25	7	240	183 mg/g	4/90	(X. Liu et al., 2019a)
Fe_3O_4 magnetic nanoparticles functionalized activated carbon (Fe_3O_4/AC)	1200	Methyl orange (MO)	0.02 g/250 mg/L	25	7	240	150 mg/g	4/94	(X. Liu et al., 2019a)
Exfoliated graphite nanoplatelets	90.08	Indosol SFGL	0.05 g/100 mg/L	25	3.5	300	104 mg/g	−/−	Carvallho et al. (2016)
Exfoliated graphite nanoplatelets	90.08	Drimaren HFRL blue	0.05 g/100 mg/L	25	3.5	300	151.2 mg/g	−/−	Carvallho et al. (2016)
S-AC1.0/MNP	2192.7	Methyl orange	10 mg/10 mL of 200 mg/L	25	2	10	869.57 mg/g	5/76	Hong et al. (2020)
ZnO: Cr-NPs-AC	–	Malachite green	0.019 g/50 mL of 4.5 mg/L	[c]r.t.	6	[d]3.9	98.36	3/-	Jamshidi et al. (2016)
ZnO: Cr-NPs-AC	–	Eosin yellow	0.019 g/50 mL of 4.8 mg/L	[c]r.t.	6	[d]3.9	97.24	3/-	Jamshidi et al. (2016)
ZnO: Cr-NPs-AC	–	Auramine O	0.019 g/50 mL of 4.7 mg/L	[c]r.t.	6	[d]3.9	99.26	3/-	Jamshidi et al. (2016)

[a] Initial concentration (mg/L).
[b] Adsorption carpacity (mg/g).
[c] r.t..
[d] Ultrasonic-assisted adsorption.

560.58 mg/g at pH 6andc308 K. The authors discovered an undesirable reasonable adsorption performance between H^+ and the positively charged cationic dye at high acidity level (Zhang et al., 2017; Hasan, 2015, 2019). In addition, the amount of positive charge on the photocatalyst composites increases at low pH, thus resulted in electrostatic repulsion between the dye molecules and is not favoring adsorption (Naseeruteen et al., 2018). Meanwhile, the color of the MG in the solution was disappears at a higher pH than 8.0. Therefore, the optimal initial pH chosen for subsequent adsorption of MG was 6.0. The adsorption behaviour of MG is in accordance to the Langmuir isotherm model and pseudo-second order kinetic equations, implies the interaction between the cationic dyes and anionic groups (phenol hydroxyl) of photocatalysts was primarily controlled by chemisorption behavior (Jiang et al., 2017; Hasan et al., 2015). The superiorities of Fe_3O_4/PT/GO towards dyes adsorption are also credited to (i) the presence of phenolic hydroxyl groups on the surface of adsorbent, which interacted with the negatively charged groups on the dye molecule $=N^+(CH_3)_2$through an electrostatic force and (ii) π-π interaction between the benzene ring and C=O on the Fe3O4/PT/GO adsorbent and the benzene ring on the dye molecule (Saeed et al., 2010). Impressively, with the assistance of magnetic separation, a number of five generation experiments were performed where the removal efficiency retained at 86% after the fifth experiment.

Jiang et al. studied the cationic dye adsorption of magnetic iron oxide/activated carbon prepared from sugarcane bagasse by microwave method, denoted as MSBAC (Jiang et al., 2021). This adsorbent is a combination of high specific surface area and porous structure for enhanced MB dye removal from aqueous solution (Thommes et al., 2015). Unlike the other reports, the solution pH in this case had a weak effect on the MB adsorption where no significant change on removal efficiency was observed by MSBAC, suggested the adsorption of MB by MSBAC was occurred by physical adsorption due to weak van der Waals forces. The adsorption results showed that the maximum adsorption capacity of MSBAC was 36.14 mg/g when the pH was fixed to 4.1 and MSBAC could regeneratively run for four cycles with a high retaination efficiency of more than 83%. Owing to its magnetic properties of MSBAC, it could be separated from the liquid phase with ease under the action of magnetic field (Fig. 3a–c) (Jiang et al., 2021).

In another work, Liu et al. enhanced the adsorption capacity of Fe_3O_4 magnetic nanoparticles entrapped with activated carbon (Fe_3O_4/AC) as an adsorbent to remove RhB and MO from aqueous solution (Fig. 4a) (Liu et al., 2019a,b). The maximum adsorption capacity at room temperature (298 K) was 182.48 mg/g and 150.35 mg/g for RhB and MO, respectively, and these values decreases with increase of temperature, imply lower temperature is more promising for dye adsorption. In addition, the maximum adsorption capacity of RhB is higher than that of MO under the same reaction parameter, attributed to the electrostatic interaction (Zhang and Kong, 2011). The authors reviewed that sole reliance on electrostatic interaction is not enough to drive the dye adsorption. Adsoption happened through hydrogen bond interaction between the adsorbent and dye molecules, as well as π-π interaction. Fig. 4b demonstrated the adsorption mechanisms of RhB (i) and MO (ii) by using Fe_3O_4/AC composite as the adsorbent. The oxygen atom of S=O group for MO molecules could be used as the hydrogen-bonding acceptor and formed intramolecular hydrogen bonding with the hydrogen atom of hydroxyl group on Fe_3O_4/AC(Ma et al., 2012). Moreover, when the adsorbent was adsorbed to RhB and MO, the presence of -COOH suggests that the carboxyl of Fe_3O_4/AC had anvital role in the electrostatic interaction attributed to the ionization, which made the adsorbent surface negatively charged. The different types of catalysts properties such as surface area (Khalil et al., 2020; Choong et al., 2019; Masoumi et al., 2017), porosity and actives sites of catalysts (Ivan-Tan et al., 2017; Haafiz et al., 2017; Chu et al., 2013) may influence on the efficiency of catalyst. In summary, considering the cost and

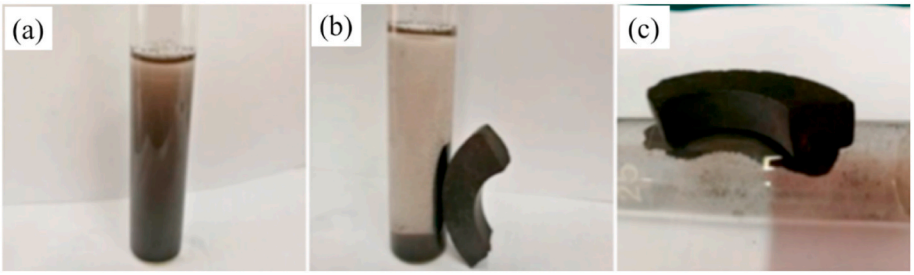

Fig. 3. (a–c) Magnetic response of MSBAC to an external magnetic (Jiang et al., 2021).

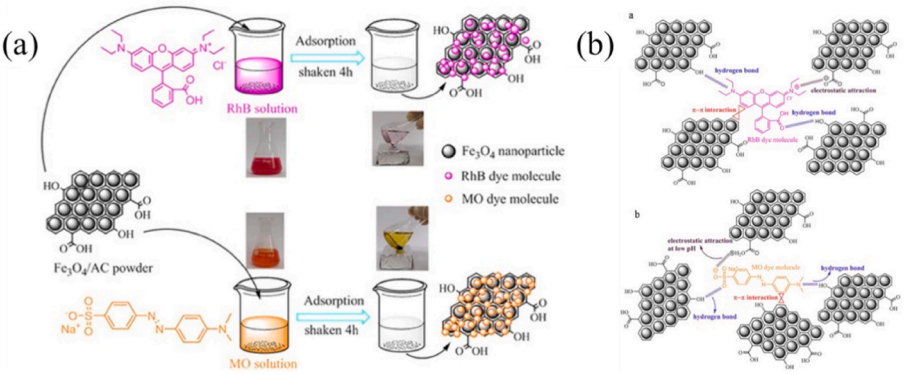

Fig. 4. (a) The application of Fe_3O_4/AC sample for removing RhB and MO from the aqueous solution. (b) adsorption mechanisms of RhB (a) and MO (b) by using Fe_3O_4/AC composite as the adsorbent (X. Liu et al., 2019a).

facile synthetic process of the Fe_3O_4/AC composite adsorbent, this adsorbent is environmental friendly and is regarded as a potential candidate for removing organic dyes and other water-based contaminants without the generation of secondary pollution (Liu et al., 2019a, b).

2.2. Metalcomposite-based adsorbent

In recent years, metal oxide-based nano-adsorbents have been widely applied in waste water treatment due to their unique properties, including large surface area, nano-size, high reactivity, high ability to blend, and robust solution mobility. Recently, Aslam and co-workers synthesized and characterized magnetic nanoparticles (cobalt-iron oxide), which are functionalized with hydrazine (CoFeNPs1) and dodecylamine (CoFeNPs2). They were used to remove various negatively charged azoic dyes such as Acid orange 7, Amaranth, reactive orange 16, reactive red-P2B, naphthol blue black, and acid orange 52 from water (Qurrat-Ul-Ain et al., 2019). The authors examined the dye

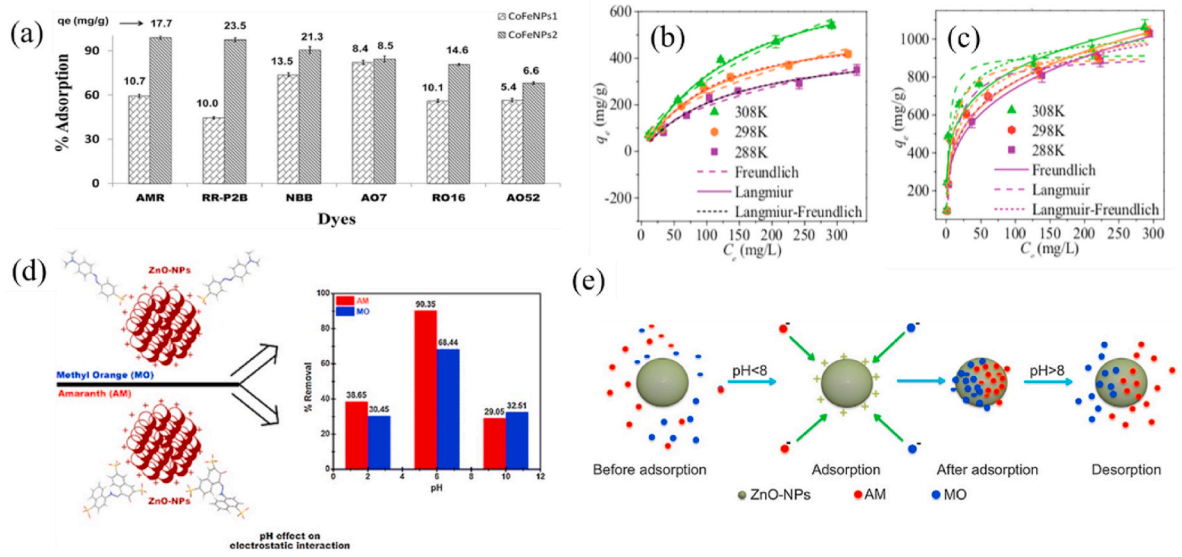

Fig. 5. (a) Comparison of the adsorption ability of CoFeNPs1 and CoFeNPs2 for six anionic azo dyes (AMR, RR-P2B, NBB, AO7, RO16, and AO52) [conditions: initial dye concentration 0.02 mmol/L, temperature 30 °C, pH 6, and adsorbent dose 0.67 g/L] (Qurrat-Ul-Ain et al., 2019), (b) adsorption isotherm of MO and (c) CR on 1Al-Fe_2O_3/LDH under different temperature at m/V = 0.2 g/L and pH 5.5 (Cheng et al., 2019), (d) effect of pH on the electrostatic interaction responsible for adsorption of dyes onto ZnO-NPs, (e) schematic representation for the possible interactions between the ZnO-NPs and AM and MO dye ions (Zafar et al., 2019).

removal efficiency by investigating the type of anchored amine, time, structure of the dye, and size of CoFeNPs. Fig. 5a shows that CoFeNPs2 has higher efficiency in removal of all dye, as compared to CoFeNPs1 with a superior dye removal efficiency up to 68–98.9% and an adsorptive capacity of 6.6–23.5 mg/g at a temperature of 3 0 C, pH 6.0, adsorbent dose of 0.67 g/L, and 20 μmol/L of dye concentration. Whilst, by functionalizing with the hydrazine, CoFeNPs1 demonstrated 44.5–82.1% dye elimination efficiencies at equilibrium (within 28–115 min) with an adsorptive capacity of 5.4–13.5 mg/g under similar circumstances. This phenomenon could be ascribed to less negative or more positive charge available on the CoFeNPs2 surface. The zeta potential values at pH 6 confirm that CoFeNPs1 is more negative than CoFeNPs2 due to better neutralization of the ferrite positive charge by free amino electrons in CoFeNPs1 (two amino groups per hydrazine coated), while CoFeNPs2 comprises single amino group per dodecylamine coated, hence confirming the effect of CoFeNPs charge on the removal of negatively charged azoic dyes. In addition, the presence of long alkyl chain in dodecylamine is hypothesized to be coated on the CoFeNPs2 surface, thus provide a platform as a basal plane for the hydrophobic interactions of CoFeNPs2 with hydrophobic groups (aromatic rings) in the dye molecules (Liu et al., 2019a,b). Moreover, the quantity of sulfur atoms in the anionic dyes is one more interesting factor that affect the dye removal ability of the catalyst (Hena et al., 2018; Hussain et al., 2019; Kamel et al., 2019; Kobayashi et al., 2020; Kubra et al., 2021a,b). The dyes exhibiting a greater number of negative charged phenyl-sulfonate (SO_3^-) moities such as AMR and RR-P2B caused in better removal ability by CoFeNPs2, hence provide more positively charged amine-functionalized adsorbents with better electrostatic attraction (Yin et al., 2017). In another work, Mahapatra et al. published a report with 416.66 mg/g of adsorption capacity for the adsorptive decolorization of CR dye using Fe_2O_3-Al_2O_3 nanohybrid catalyst at pH 7.0. The authors inferred that the excellent adsorption capacity was attributed to the interaction between amine functional groups of the CR dye molecules with the oxy-hydroxide group of the nanohybrid material (Dutta et al., 2021; Marwani et al., 2017; Rahman et al., 2018; Sheikh et al., 2016; Shenashen et al., 2020; 2021; 2021a).

Meanwhile, Cheng et al. synthesized innovative Al-doped iron oxides decorated layered double hydroxides nanocomposite (Al-Fe_2O_3/LDH) by one-spot hydrothermal reaction (Cheng et al., 2019). The presence of LDH nanoflakes as a matrix mediates the assemble of oxides nanoparticles, thus contributed to high adsorption capacities (1363.54 mg/g and 577.42 mg/g) for Congo red (CR) and MO, respectively. The good dispersion of 1Al-Fe_2O_3/LDH and the synergism between layered hydroxide nanoflakes and supported Al-doped iron oxides contributed to a fast and enhanced removal ability. The adsorption isotherm of CR was best fitted by Langmuir-Freundlich model, suggesting the CR molecules adsorbed on the multi-layer adsorbent and both chemical and physical interactions are happened between catalyst and pollutants. While the MO was best fitted by Langmuir model, implies MO molecules were localized in a monolayer mode of 1Al-Fe_2O_3/LDH surface. Both the kinetics were well fitted by pseudo-second-order, indicative of dominant chemical adsorptions on 1AL-Fe_2O_3/LDH heterogeneous surface (Fig. 5b–c) (Lei et al., 2017; Li et al., 2016). In another work, Zafar et al. reported that nanostructured ZnO adsorbent displayed remarkable efficiency toward dyes removal, including MO and amaranth (AM) from aqueous solutions (Zafar et al., 2019; Suzuki et al., 2014, 2015; Taguchi et al., 2014, 2016). Results showed that the removal of MO increased up to 90% at pH 6.0 and the removal of AM increases to 95% at pH 7.0. Since the maximum elimination was found at pH 6.0 and 7.0 for MO and AM, respectively, the dominant adsorption mechanism is mainly by electrostatic attraction between the anionic dyes molecules and positively charged ZnO-NPs (pH PZC = 9.8), as shown in Fig. 5c. The pH below PZC of the ZnO-NPs caused them positively charged which enhanced electrostatic attraction between dye and ZnO surface (Salem et al., 2016). The adsorption investigations proved that the adsorption process of both dyes is strongly persisting to Langmuir model and both the adsorption processes were pseudo-second-order (Toyohara et al., 2020; Yaita et al., 2013, 2015; Znad et al., 2021, 2021a; Roy et al., 2022). Analyses proved that the adsorption process of MO and AM dyes was attributed to the chemical action between ZnO-NPs based adsorbents and anionic dyes where electrostatic interactions exerted between the negative charged moities on anionic dyes and positive charge groups at ZnO-NPs (Fig. 5d). From the practical point of view, the dye charged on ZnO-NPs could be reactivated using low concentration of alkali in ethanol solution and pure ethanol, implies ZnO-NPs are cost-effective adsorbents for future water treatment. Table 3 presents the performance of metal and metal oxide-based hybrid nanocomposites as adsorbents used in dye removal.

2.3. Gel-based adsorbent

The development of hydrogels has shown promised performances toward purify dyes-contaminated effluents ascribed to their high adsorption capacity, reusability, low cost and ease operando. Hydrogel is a three-dimensional (3D) cross-linked polymeric material that is capable of absorbing huge amount of water without dissolving, particularly in removing dyes in wastewater through adsorption mechanism (Khan and Lo, 2016). The activity of polymer and gel-based adsorbent for the degradation of dyes is shown in Table 4. Nevertheless, the conventional uncross-linked poly (acrylic acid) (PAA) adsorbent exhibits low dyes adsorption capacity owing to the poor 3D bulk structure that induces the penetration of water into the internal channels of the adsorbent. For this reason, Bello et al. (2018) synthesized an environmental friendly superabsorbent hydrogel derived from banana pseudo-stem via free radical graft co-polymerization using ammonium persulfate (APS) and N,N-methylene-bis-acrylamide (MBA) as the initiator and crosslinker, respectively(Bello et al., 2018; Saleh et al., 2020). Fig. 7a despicts the proposed mechanism for graft copolymerization. The synthesized hydrogel, named as BPCMC-g-poly (NaAc-*co*-AM) possesses abundant functional groups (C-O, C-H, O-H, RCOH, N-H, etc.), highly porous and its undulant surface promotes the penetration of dyes into the polymer network (Fig. 6a), thus garnered maximum adsorption capacity of 333.3 mg/g for cationic MB dyes and 124 mg/g for anionic methyl orange (MO) dyes at pH 7.0 (Bello et al., 2018). The anionic based superabsorbent hydrogel containing hydrophilic carboxyl and carboxamide groups and is highly sensitive to pH. Evidently, an acidic medium exhibited milder swelling ratio owing to the formation of hydrogen bonding between COOH (from protonation of COO-), and NH_2 groups, hence cause the shrinkage of hydrogel. Moreover, a facile and efficient microwave irradiation method was adopted by Pandey and co-workers for the synthesis of XG-cl-pAA/rGO hydrogel composite (Makhado et al., 2018). XG is this work is referred to xanthan gum, which is an efficient polyelectrolyte due to the presence of tunable hydroxyl (-OH) groups. The presence of hydrophilic oxygenated functional groups on the surface or edge of rGO sheets have substantially improved the swelling capacity of XG-cl-pAA/rGO hydrogel, which is in agreement with the results reported in literature (Huang et al., 2012). Different amount of rGO were added into the hydrogen matrix and it shows that the highest content of 80 mg rGO leads to the highest percentage of adsorption, ascribed to the negatively charged groups of rGO (COO^-) that attract the positively charged dyes interactions. In addition, the formation of rough and folded with more defined porous structures of XG-cl-pAA/rGO hydrogel, as shown in Fig. 6b, would facilitate and fasten the uptake of pollutants such as MB and methyl violet (MV) dyes. Evidently, the adsorption of MB and MV altered the shape and size of the hydrogel morphologies (Fig. 6c–d), thus proved the loading of dyes onto the surface of hydrogel (Makhado et al., 2018).

Realizing the effectiveness of graphene-based hydrogel in adsorption process, Chen et al., have successfully developed a three-dimensional network structure of konjac glucomannan/graphene oxide (KGM/GO) sponges via ice template method for MG dye removal (Fig. 7a) (Chen et al., 2018). The reason of using KGM as one of the raw materials is due

Table 3
Different composite of metals for the degradation of dyes.

Catalyst	Pollutant	Loading (catalyst/[a]pollutant)	Reaction conditions			Efficiency (%)	Regeneration (cycles)	Ref.
			T (°C)	pH	T (min)			
Cobalt–iron oxide nanoparticles functionalized hydrazine (CoFeNPs1)	Amaranth	0.67 g/12.1 mg/L	30	6	53	[b]11 mg/g	–/–	Qurrat-Ul-Ain et al. (2019)
Magnetic cobalt–iron oxide nanoparticles functionalized dodecylamine (CoFeNPs2)	Amaranth	0.67 g/12.1 mg/L	30	6	115	[b]8 mg/g	–/–	Qurrat-Ul-Ain et al. (2019)
Cobalt–iron oxide nanoparticles functionalized hydrazine (CoFeNPs1)	Red-P2B	0.67 g/15.8 mg/L	30	6	40	44.5	–/–	Qurrat-Ul-Ain et al. (2019)
Cobalt–iron oxide nanoparticles functionalized dodecylamine (CoFeNPs2)	Red-P2B	0.67 g/15.8 mg/L	30	6	150	97.5	–/–	Qurrat-Ul-Ain et al. (2019)
Cobalt–iron oxide nanoparticles functionalized hydrazine (CoFeNPs1)	Naphthol Blue Black	0.67 g/12.3 mg/L	30	6	105	[b]14 mg/g	–/–	Qurrat-Ul-Ain et al. (2019)
Cobalt–iron oxide nanoparticles functionalized dodecylamine (CoFeNPs2)	Naphthol Blue Black	0.67 g/12.3 mg/L	30	6	162	[b]21 mg/g	–/–	Qurrat-Ul-Ain et al. (2019)
Magnetic cobalt–iron oxide nanoparticles functionalized hydrazine (CoFeNPs1)	Acid Orange 7	0.67 g/7 mg/L	30	6	105	[b]8 mg/g	–/–	Qurrat-Ul-Ain et al. (2019)
Cobalt–iron oxide nanoparticles functionalized dodecylamine (CoFeNPs2)	Acid Orange 7	0.67 g/7 mg/L	30	6	150	[b]9 mg/g	–/–	Qurrat-Ul-Ain et al. (2019)
Cobalt–iron oxide nanoparticles functionalized hydrazine (CoFeNPs1)	Reactive Orange 16	0.67 g/-	30	6	30	[b]68 mg/g	–/–	Qurrat-Ul-Ain et al. (2019)
Cobalt–iron oxide nanoparticles functionalized dodecylamine (CoFeNPs2)	Reactive Orange 16	0.67 g/-	30	6	75	[b]74 mg/g	–/–	Qurrat-Ul-Ain et al. (2019)
Cobalt–iron oxide nanoparticles functionalized hydrazine (CoFeNPs1)	Acid Orange 52	0.67 g/6.5 mg/L	30	6	28	[b]5 mg/g	–/–	Qurrat-Ul-Ain et al. (2019)
Cobalt–iron oxide nanoparticles functionalized dodecylamine (CoFeNPs2)	Acid Orange 52	0.67 g/6.5 mg/L	30	6	93	[b]7 mg/g	–/–	Qurrat-Ul-Ain et al. (2019)
γ-Fe2O3-Al2O3	Congo red	0.1 g/100 mg/L	[c]r.t.	7	15	[b]498 mg/g	–/–	Mahapatra et al. (2013)
Al-Fe2O3/LDH	Congo red (CR)	0.005 g/10 mg/L	25	5.5	30	[b]1364 mg/g	4/-	Cheng et al. (2019)
Al-Fe2O3/LDH	methyl orange (MO)	0.005 g/10 mg/L	25	5.5	30	[b]577 mg/g	4/-	Cheng et al. (2019)
ZnO	Methyl orange (MO)	0.3 g/40 ppm	55	6	50	[b]90 mg/g	4/60	Zafar et al. (2019)
ZnO	Amaranth (AM)	0.3 g/40 ppm	55	6	50	[b]68 mg/g	4/78	Zafar et al. (2019)
Ag2S@Ag	Methylene blue	7.58 mg/10 mL of 60 mg/L	–	–	5	[b]99.83	–/–	Zhang et al. (2016)
ZnO@Ze	Congo red	0.05 g/50 mL of 300 mg/L	32	3	20	[b]161 mg/g	5/90	Madan et al. (2019)
Ag–Cu@ZnO	Rhodamine B	5 mg/1 ml of 10 mM	–	–	0.2	99	4/>90	Manjari et al. (2020)
Ag–Cu@ZnO	Rhodamine B	5 mg/1 ml of 10 mM	–	–	0.15	99	4/>90	Manjari et al. (2020)
κ-Carrageenan/Ag	Rhodamine B	—/100 ppm	–	–	0.25	99	3/~90	Pandey et al. (2020)
NH2-MIL-101(Fe)@CuCoNi	Methylene blue	50 mg/25 mg/L	30	3	120	99	5/83.1	Chen et al. (2020)
NH2-MIL-101(Fe)@CuCoNi	Crystal violet	50 mg/25 mg/L	30	3	120	93	5/90	Chen et al. (2020)
Si/Cu amorphous	Methylene blue	100 mg/150 mg/L	25	8	60	[b]102 mg/g	4/-	Hameed (2020)
SnO2QDs	Rhodamine B	0.25 g/40 mg/L	–	4	180	90	–/–	Fatimah et al. (2020)
CdS/SnO2 NPs	Methylene blue	0.1 g/100 mL of 2 × 10−5 mol/L	30	–	180	90	5/83	El-Katori et al. (2020)
SnO2-SnS2	Methylene orange	50 mg/50 mL of 10 mg/L	–	–	60	~99	4/>90	Yadav et al. (2020)

[a] Initial concentration (mg/L).
[b] Adsorption carpacity (mg/g).
[c] r.t..

to it is a renewable natural polymer with high molecular weight polysaccharide composed of β-1,4 linked D-mannose and D-glucose with acetyl groups attaching randomly to C-6 position and possesses a large number of hydroxyl groups in the polymer chain. By coupling with the GO, noncovalent interaction and covalent crosslinking (hydrogen bonding and conjugation) between KGM and GO, thus gave rise to superior physicochemical properties. Experimental results showed that the adsorption of MG on the sponges was monolayer with an adsorption capacity of 189.96 mg/g for the KGM/GO hydrogel and 57.37 mg/g for KGM, implies the applicability of KGM/GO sponges in catalysis and other fields (Yao et al., 2012). In another work, Hu et al. (2018) utilized non-aggregated calcium hydroxide nano-spherulites (CNS) as the cross-linkers to prepare a novel PAA-based super-adsorbent nanocomposite hydrogen, denoted as NC gel via free radical in-situ polymerization (Fig. 7b). The NC gel adsorbent possesses inter-penetrating channels within internal porous structure which provides excellent adsorption sites of adsorbent towards dyes and thus contributed to a high maximum adsorption capacity of 2100 mg/g at a near neutral pH of 7 towards the removal of methylene blue (MB). The high adsorption capacity of the NC gel adsorbent is closely related to the synergistic effect of electrostatic interactions and hydrogen bonds between NC gel and MB, which is one of the main factors that affect the adsorption behavior under different pH of MB medium. Evidently, in an acidic medium (pH 1–5), the protonation of COO^- to COOH groups of polymer chains is unfavourable for adsorption attributed to the less hydrogen bonds formed between NC gel and MB. Meanwhile, at base pH of 9–13, the ionization of COOH to COO^- causes the breakdown of hydrogen bonding interaction and charge screening effect of excess Na^+ ions result in ineffective electrostatic attractions between COO^- of polymer and MB. At a neutral condition, the moderate residual COO- and COOH

Table 4
Polymer and gel-based adsorbent for the degradation of dyes.

Catalyst	Surface area (m2/g)	Pollutant	Loading (catalyst/[a]pollutant)	Reaction conditions			Efficiency (%)	Regeneration (cycles)	Ref.
				T (°C)	pH	T (min)			
BPCMC-g-poly (NaAc-*co*-AM)	–	Methylene blue (MB)	16 mg/50 mg/L	[c]r.t.	7	570	[b]333 mg/g	3/96	Bello et al. (2018)
BPCMC-g-poly (NaAc-*co*-AM)	–	Methyl orange (MO)	16 mg/50 mg/L	[c]r.t.	7	570	[b]124 mg/g	3/92	Bello et al. (2018)
XG-cl-pAA/rGO	–	Methyl violet (MV)	10 mg/-	25	5	60	[b]1053 mg/g	4/~96	Makhado et al. (2018)
XG-cl-pAA/rGO	–	Methylene blue (MB)	30 mg/-	25	5	30	[b]794 mg/g	4/>95	Makhado et al. (2018)
Konjac glucomannan/graphene oxide (KGM/GO) sponges	–	Malachite green	10 mg/30 mg/L	40	<2	100	[b]190 mg/g	5/~160	Chen et al. (2018)
Poly(acrylic acid) (PAA) based Calcium hydroxide nano-spherulites (CNS)	–	Methylene blue (MB)	1g/100 mg/L	25	7	420	[b]2100 mg/g	5/-	Hu et al. (2018)
SNF/HAP	0.962	Au(III)	0.2 wt%/150 mL of 100 mg/L	–	–	–	[b]164 mg/g	−/−	Ling et al. (2021)
CNF-PdNPs	–	Congo red	2 mL/20 mg/L	–	–	30	100	5/>91	Gu et al. (2018)
CNF-PdNPs	–	Methylene blue	2 mL/20 mg/L	–	–	3	100	5/>99	Gu et al. (2018)
Fine aminated cellulose/montmorillonite mesoporous composite beads (ACeMt)	46	Auramine O	0.5 g/L/100 mL of 80 mg/L	55	7	–	[b]1336 mg/g	5/>20	Pan et al. (2019)
Fine aminated cellulose/montmorillonite mesoporous composite beads (ACeMt)	46	Amido black 10B	0.5 g/L/100 mL of 50 mg/L	35	3	–	[b]232 mg/g	5/>20	Pan et al. (2019)
Fe3O4/AC/CD/Alg	8	Methylene blue	0.2 g/5 ppm	[c]r.t.	6	90	99.5	5/89.26	Sunaina et al. (2020)
PANI/PVAL/F	–	Reactive Black 5	50 mg/50 mL of 55 mg/L	[c]r.t.	–	240	99	−/−	Bober et al. (2020)
MBCNF/GOPA	214.75	Malachite green	50 mg/30 mg/L	25	7	25	82	8/>62	Arabkhani and Asfaram (2020)
PVA/CH/AgNPs	–	Bacterial	–	37	–	24	91.8	–	Kumar and Kaur (2020)
SSF	–	K-2BP	10 g/20 mL of 0.25 g/L	–	0.3	2	98.6	3/~1000 mg/g	Wang et al. (2021)
CCF	29.21	Eosin Y	10 mg/20 mL of 20 mg/L	25	7.2	120	99.5	8/>60	Feng et al. (2020)
PANP(−)F	–	Brilliant cresyl blue	10 mg/40 mL of 1 mmol/L	25	10	180	179 mg/g	10/95.8	Xiao et al. (2020)
Ag3PO4/GO/APTES/PVDF	–	Methylene blue	—/20 mg/L	–	–	–	89	3/-	(R. Zhang et al., 2020a)
Ag3PO4/GO/APTES/PVDF	–	Rhodamine B	—/10 mg/L	–	–	–	85	3/-	(R. Zhang et al., 2020a)
P(AA-co-AMPS) hydrogel spheres	–	Methylene blue	3 mg/20 mL of 1000 μmol/L	–	7	–	[b]4463 mg/g	5/79.63	Yin et al. (2020)
P(AA-co-AMPS) hydrogel spheres	–	Pb(II)	3 mg/20 mL of 20 μmol/L	–	7	–	[b]6393 mg/g	–	Yin et al. (2020)
Ag NPs@MIL-100(Fe)/GG	–	Methylene blue	—/40 mL of 40 mg/L	–	4	100	100	–	(Chao Duan et al., 2020)
CNF/PEI/Ag NPs	<3.5	Methylene blue	—/40 mL of 10 mg/L	–	–	5	100	10/>98	(W. Zhang et al., 2020b)
CNF/PEI/Ag NPs	<3.5	Congo red	—/40 mL of 10 mg/L	–	–	21	100	–	(W. Zhang et al., 2020b)
Surface-engineered sponge (SEnS)	11.12	Crude oil	0.85 g/9500–10000 mg/L	40	5.6	10	92	10/99	Cherukupally et al. (2020)

[a] Initial concentration (mg/L).
[b] Adsorption carpacity (mg/g).
[c] r.t..

groups are conducive for the formation of electrostatic interactions and hydrogen bonds between NC gel and MB, which gave rise to an optimal performance (Hu et al., 2018). This work reflects the importance of choosing suitable crosslinkers that help to consolidate the hydrogel framework, consequently enhance the adsorption performance.

2.4. Photocatalyst-based adsorbent

Photocatalytic degradation is an alternative technique that offers an eco-friendly and sustainable treatment process to the water bodies where the organic dyes from waste water could be completely degraded by the photocatalysts with excellent oxidation ability, such as TiO_2, ZnO, CdS, Fe_2O_3, WO_3, etc. (Ikram et al., 2020a, 2020b). It usually happens within few hours at room temperature when a semiconductor photocatalyst absorbs sunlight and completely break down the organic pollutants to relatively non-hazardous products such as water and CO_2. Typically, the photocatalyst yields hydroxyl radicals (·OH), subsequently react with liquid dissolved organic dyes and convert them into organic small molecules with low toxicity such as H_2O and CO_2 at a milder temperature and pressure without the need of oxidants (Wang et al., 2012). An efficient process in eliminating dyes in both reactions is highly dependent on the surface area of the materials used (Sandoval

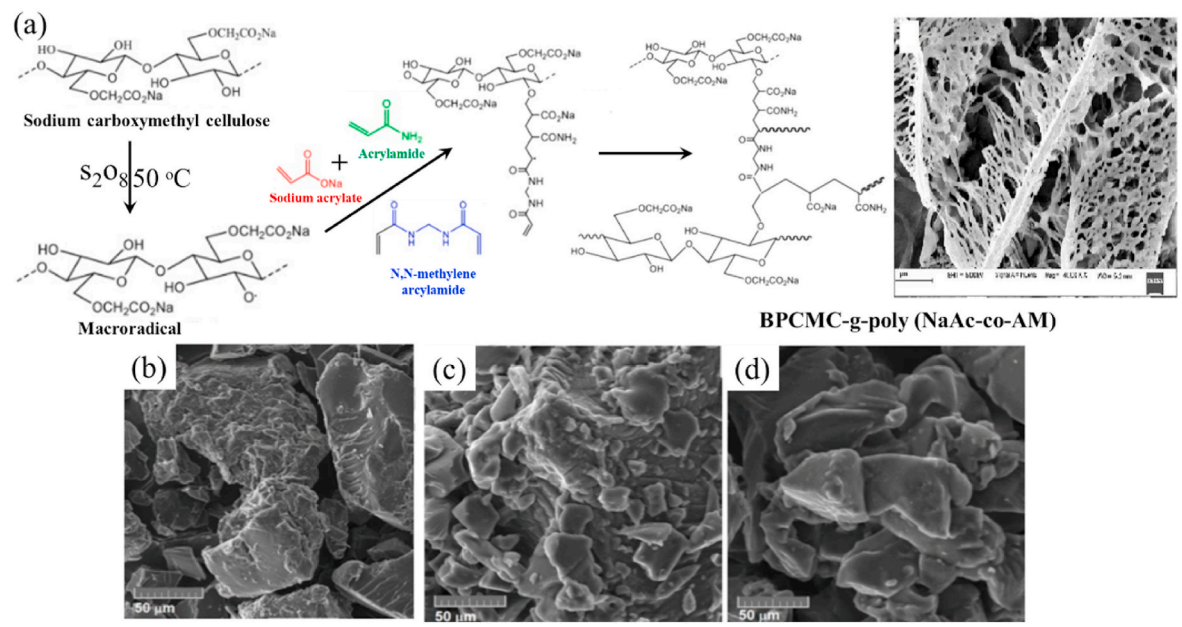

Fig. 6. (a)Proposed reaction mechanism for APS initiated graft copolymerization of poly (NaAc-*co*-AM) on BPCMC and SEM image of BPCMC-*g*-poly (NaAc-*co*-AM) (Bello et al., 2018), SEM images of (b) XG-cl-p(AA)/rGO hydrogel composite, (c) MB loaded XG-cl-p(AA)/rGO, and (d) MV loaded XG-cl-pAA/rGO(Makhado et al., 2018).

et al., 2017). Additionally, surface functionalization of the nanomaterials is the next important factor that could bond to the dye molecules, subsequently decomposing them by reactive radicals (M Ikram et al., 2020). The adsorption of dye molecules on the surface of photocatalyst is usually influenced by several parameters such as initial dye concentration, pH of the solution, irradiation intensity, and reaction temperature (Rafiq et al., 2021). For these reasons, several research groups have explored numerous methods to tackle dye-contaminated wastewater using various kinds of photocatalysts (Cai et al., 2020a,b; Kusior et al., 2019; Yang et al., 2019). The activity of photocatalyst based composite for the degradation of dyes is shown in Table 5.

Among the mentioned photocatalysts, TiO_2 has been well-established for water purification, environmental protection, and photocatalysis owing to its availability, corrosion resistance, nontoxicity, porous surface nanomorphology, and excellent photostability (Fujishima and Zhang, 2006; Lai and Sreekantan, 2013a; Zhang et al., 2008). Nevertheless, large band gap of TiO_2 (~3.0–3.2 eV) limits the sunlight absorption higher than ultraviolet region, making it impractical for real application (Sridharan et al., 2013). As a solution to this problem, TiO_2 is coupled to another semiconductor metal oxide with a suitable band gap, which prompts for an improved TiO_2 photocatalytic activity and decreasing electron-hole pair's recombination (Malato et al., 2009). For instance, mesoporous WO_3/TiO_2 photocatalysts with different loadings of WO_3 were prepared to eradicate MB from the aqueous solution (Fig. 8a) (El-Yazeed and Ahmed, 2019). The combination of a large band gap TiO_2 and a narrower band gap WO_3 (2.4–2.8 eV) with different energy levels increases charge separation and is responsive to visible light (more than 12%) (Lai and Sreekantan, 2013b; Stojadinović et al., 2012). With an appropriate energy level between both semiconductors, the photoexcited electrons in the conduction band of TiO_2 will be efficiently transferred to WO_3, whilst the holes are transferred from the valence band of WO_3 to the valence band of TiO_2 in an opposite pathway, thus inhibit charge recombination and enhance the photodegradation mechanism. At this point, the holes of the valence band can be easily reacted with the adsorbed H_2O or OH^- to generate hydroxyl radicals (OH·) (Ismail et al., 2016). On the other hand, the photogenerated electrons on the WO_3 sites would be reduced from $W6^+$ into $W5^+$ and can be reoxidized into $W6^+$ by O_2 that was reduced into the superoxide radical anion ($O_2{\cdot}^-$). The produced OH·, $O_2{\cdot}^-$and $HO_2{\cdot}$ are responsible for the photodegradation process (Grbić et al., 2014; Han et al., 2018; Ma et al., 2014). In another work reported, Han et al., modified the band gap of mesoporous TiO_2 with WO_3 by immersing mesoporous TiO_2 nanoparticles in the peroxotungstic acid sol with controllable reaction time (Han et al., 2018). In order to study the influence of WO_3 content on the photoactivity of TiO_2, the mesoporus-TiO_2 (M-TiO_2) was dipped in sol by varying the immersing durations. BET results show that the photocatalyst immersed for 0.5 h (0.5h-WO_3/RM-TiO_2) exhibited the largest pore volume of 0.491 cm^3g^{-1} and the highest surface area of 82.3 m^2g^{-1}, thus resulted in an excellent degradation mechanism. This phenomenon could be ascribed to an appropriate content of WO_3 was loaded onM-TiO_2 for an immersion duration of 0.5h, thus induces the lowest resistance for electron transfer and excellent charge separation process. Unlike the higher immersion duration of more than 0.5 h, excessive growth of WO_3 around M-TiO_2 plunges the surface area by blocking the channels of M-TiO_2 (Zhan et al., 2017).

Apart from the mature TiO_2, other kinds of photoactive catalysts are also emerging, including carbon-based materials and ZnO. Taking an example of reduced graphene oxide (rGO), Siong et al. proved that rGO exhibits excellent adsorption properties and photoactivity towards removal of MB dye (Siong et al., 2019). The rGO was prepared through solvothermal approach where the GO dispersion was reduced into rGO at different temperatures (80, 120, 160, and 180 °C) for 2 h in a Teflon-lined stainless-steel autoclave. Temperature control in this case is important because GO reduction is insufficient at low reduction temperatures. Meanwhile a high reduction temperature of 180 °C may plunge the surface area of rGO, thus reduce the amount of dye adsorbed. The highest photoactivity (32.68%) was exhibited by rGO-160, as demonstrated in Fig. 8b–c, where dye molecules are well-interacted with the reactive oxygen species when they were adsorbed on the surface (He et al., 2018). The enhancement of photoactivity at an optimum solvothermal temperature of 160 °C could be also ascribed to the partial restoration of sp^2-hybridized structure of graphene and the substantial removal of surficial oxygen functionalities. In addition, the authors added that optimizing the parameters such as catalyst amount, initial dye concentration, light intensity, and pH solution are also important to

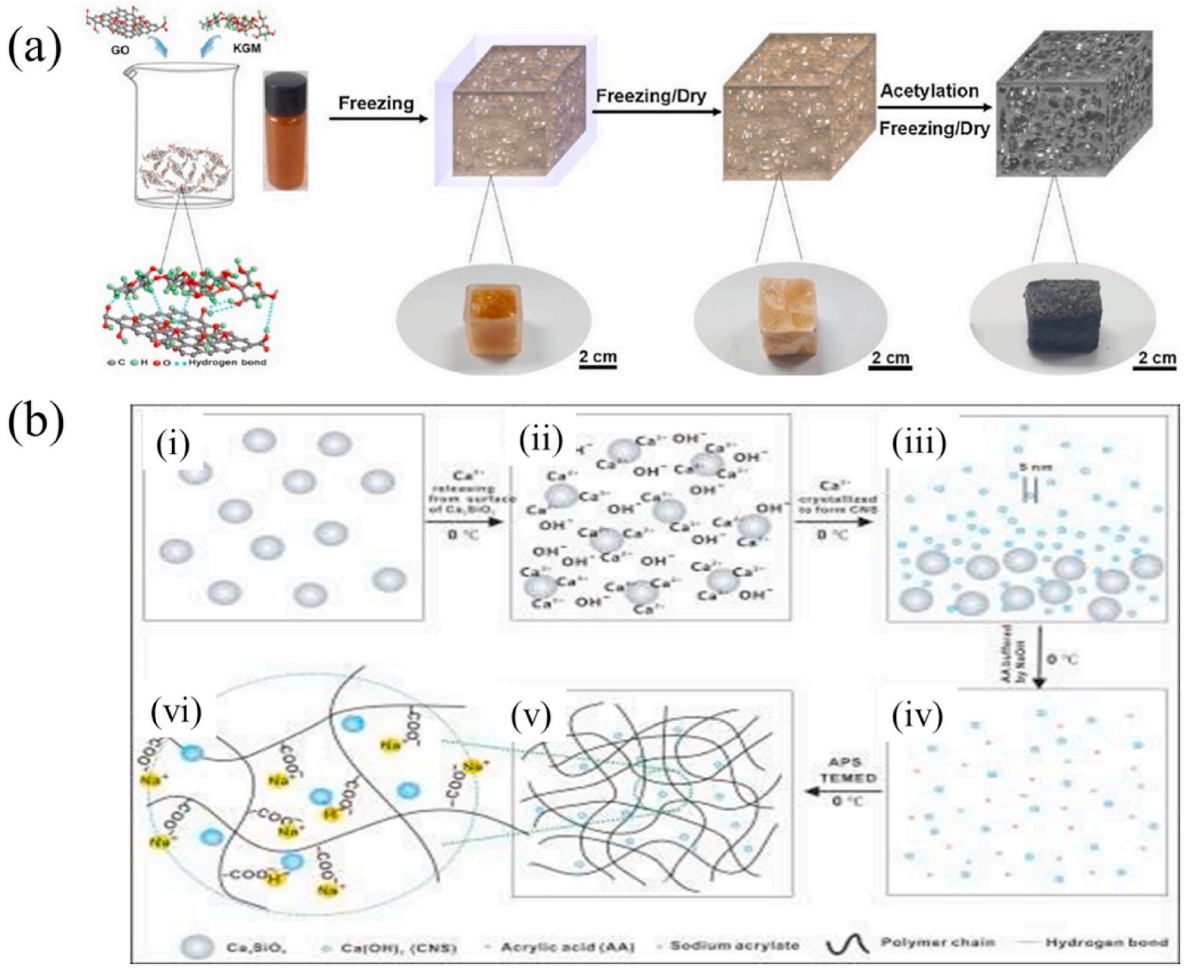

Fig. 7. (a) Schematic illustration of the fabrication of KGM/GO sponges (Chen et al., 2018) and (b) Schematic diagram of NC gel adsorbent. (i) Tricalcium silicate (Ca_3SiO_5) were dispersed in water at 0 °C and maintained at 0 °C for 3 days; (ii) Ca^{2+} released from the surface of Ca_3SiO_5 powders; (iii) Ca^{2+} crystallized to form calcium hydroxide nano-spherulites (CNS) eith diameters around 5 nm; (iv) acrylic acid, sodium acrylate and CNS were mixed uniformly; (v & vi) formation of super-adsorbent NC gel using CNS as cross-linker. The hydrogen bonds between residual -COOH groups of polymer chains and oxygen-containing functional group of CNS were responsible for the well-cross-linked network structure of hydrogel (Hu et al., 2018).

guarantee a desirable photodegradation process (Siong et al., 2019). In spite of that, nano-carbon could serve as a template for the growth of 3D honeycomb-structured ZnO nanomaterials.To ensure the successful growing of 3D honeycomb-structured, different C:Zn molar ratios were investigated by Zheng et al. (2019). Interestingly, a highly porous and thin pore wall of 3D honeycomb-structured is only formed at the molar ratio of 1:1, as illustrated in the SEM image of Fig. 8d. The authors noticed that an excessive usage of zinc acetate would destruct the honeycomb-like porous structure and cause aggregation (Fig. 8e). Therefore, ZnO prepared at molar ratio of 1:1 is expectedly exhibiting the best photocatalytic degradation behavior with a degradation rate of MB up to 95% within 90 min, credited to the thin pore walls, porous, high surface area with abundant surface-active sites.

As an alternative to further strengthen the photocatalytic performance of the ZnO photocatalyst, noble metals such as Pd, Pt, Au, and Ag could be loaded on the catalyst surface (Mohammadzadeh Kakhki et al., 2017; Rodrigues et al., 2020; Yu et al., 2016; Zayed et al., 2019). For example, Ag is an abundant and economical metal, as compared to Au and Pt. The deposition of Ag nanoparticles (Ag NPs) on the surface of photocatalyst is not merely effectively suppressing charge carriers' recombination, but the surface plasmon resonance effect of Ag NPs could significantly improve the adsorption of visible light. In the work reported by Park and co-workers, the authors first synthesized morphology-controlled ZnO structures through hydrothermal method by varying the NaOH concentration because the OH^- ions are the main factor that influence the growth of ZnOstructures (Ahmed et al., 2014; Lim et al., 2021; Guediri et al., 2020). The NaOH concentration varied from 0.2 to 1.2 M resulted in the formation of ZnOstructures in shapes of walnut, spherical flower, flower, rod, and urchin-like, as shown in Fig. 9a–e. Among these ZnO structures, ZnO spherical flower-like (ZnOsf) structure exhibited the greatest percentage of photodegradation toward MO and rhodamine B dyes (Fig. 9f–g). When Ag NPs were loaded on ZnOsf, the Ag-ZnOsf absorption intensity was significantly quenched, indicating lower recombination of electron-hole pairs, as compared to that of bare ZnOsf. Expectedly, the percentage degradation afforded by Ag-ZnOsf is much superior than the pristine where the Ag-ZnOsf composite degraded both MO and RhB within 35 min with 99.3% degradation percentage (Fig. 9h–i). This enhancement could be ascribed to the SPR effect of Ag NPs which significantly improved visible light absorption. In addition, it is hypothesized that ZnOsf possesses higher surface area, thus improved light absorption efficiency of the photocatalyst (Li et al., 2019). Lastly, textile derived energy/bioethanol production could be sustainable option for waste management (Mondal et al., 2021; Monir et al., 2021; Lway Faisal Abdulrazak et al., 2021). The production of the energy from waste depends on the properties of catalyst (Moniruzzaman et al., 2014; Syazwani et al., 2017). A conclusion has been reached by Wang et al. (2019) that textile sluge and biowaste could be used for the production of biochar.

Table 5
Photocatalyst based composite for the degradation of dyes.

Catalyst	Surface area (m2/g)	Pollutant	Loading (catalyst/p[a]ollutant)	Reaction conditions				Lamp (Watt)	Efficiency (%)	Regeneration (Cycles)	Ref.
				T (°C)	pH	T (min)	Additive				
Mesoporous WO3/TiO2 nanocomposites	37.21	Methylene blue (MB)	0.03 g/10 ppm	–	–	180	–	Halogen (400)	99	3/84.6	El-Yazeed and Ahmed (2019)
C-paints/water/Mn-TiO2	–	Rhodamine B	—/3 mg/L	–	–	70	–	UV (4), Xenon (150)	~100	–	Park et al. (2015)
C-paints/water/Mn-TiO2	–	Rhodamine B	—/5 mg/L	–	–	70	–	UV (4), Xenon (150)	~100	–	Park et al. (2015)
TiO2/PVDF nanofibers	–	Reactive black 5	20 mg/10 mL of 10 ppm	–	–	360	–	LED (18)	80	–	Lou et al. (2019)
Go/rGO	94.81	Methylene blue (MB)	60 mg/50 ppm	–	11	600	–	UV-C (60 W m-2)	96	5/>90	Siong et al. (2019)
Br- g-C3N4/rGO	63.1	Reactive Blue-19	0.1 g/100 mL of 10 ppm	–	–	120	–	Tungsten (500)	92	4/92	[HH] Kasinathan et al., 2020
Br- g-C3N4/rGO	63.1	Methyl Orange	0.1 g/100 mL of 10 ppm	–	–	120	–	Tungsten (500)	85	4/85	Kasinathan et al. (2020)
Br- g-C3N4/rGO	63.1	Rhodamine-B	0.1 g/100 mL of 10 ppm	–	–	120	–	Tungsten (500)	95	4/95	Kasinathan et al. (2020)
3D honeycomb-structured ZnO	–	Methylene blue (MB)	1 mg/0.6 mg/L	–	–	90	–	Mercury (100)	95	–/–	Zheng et al. (2019)
HPF-like g-C3N4/FeOCl	25.08	Tetracycline	20 mg/100 mL of 50 mg/L	30	–	20	H2O2	Xenon (300)	90	–	Zhao et al. (2020)
HPF-like g-C3N4/FeOCl	25.08	Rhodamine B	20 mg/100 mL of 10 mg/L	20	–	60	H2O2	Xenon (300)	90	–	Zhao et al. (2020)
K-doped g-C3N4/BiOBr	12.18	Rhodamine B	50 mg/50 mL of 20 mg/L	–	–	90	–	Xenon (500)	99	5/90	Qu et al. (2020)
K-doped g-C3N4/BiOBr	12.18	Tetracycline	50 mg/50 mL of 20 mg/L	–	–	150	–	Xenon (500)	>80	–	Qu et al. (2020)
ZnO spherical flower-like (ZnOsf)	13.45	Methyl orange	40 mg/10 mg/L	–	8.7	35	–	Xenon-UV-Vis	93	10/80	Lim et al. (2021)
ZnO spherical flower-like	13.45	Rhodamine B	40 mg/10 mg/L	–	8.8	35	–	Xenon-UV-Vis	93	10/80	Lim et al. (2021)

[a] Initial concentration (mg/L).

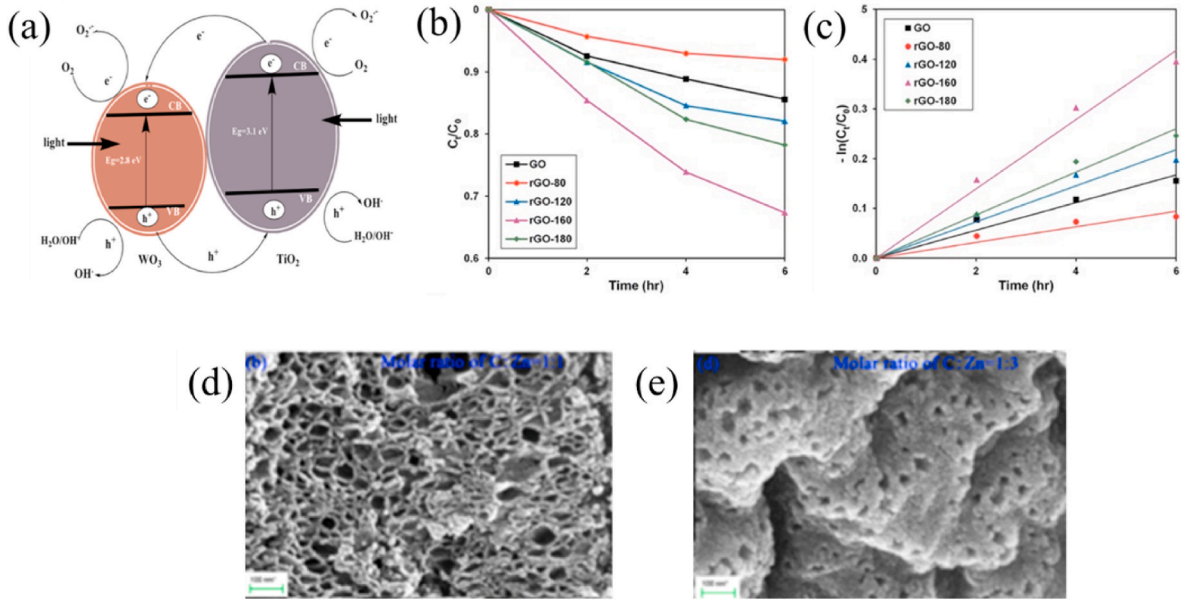

Fig. 8. (a) The photodegradation of MB using photoexcited WO_3/TiO_2 photocatalysts (El-Yazeed and Ahmed, 2019). (b) Photocatalytic degradation of MB dye normalized against adsorption, (c) Pseudo-first order kinetic plot of MB dye in the presence of GO, rGO-80, rGO-120, rGO-160, and rGO-180 (Siong et al., 2019). (d) SEM image of 3D honeycomb-structured ZnO nanomaterials at C: Zn ratio of 1:1, (e) SEM image of 3D honeycomb-structured ZnO nanomaterials at C:Zn ratio of 1:3 (Zheng et al., 2019).

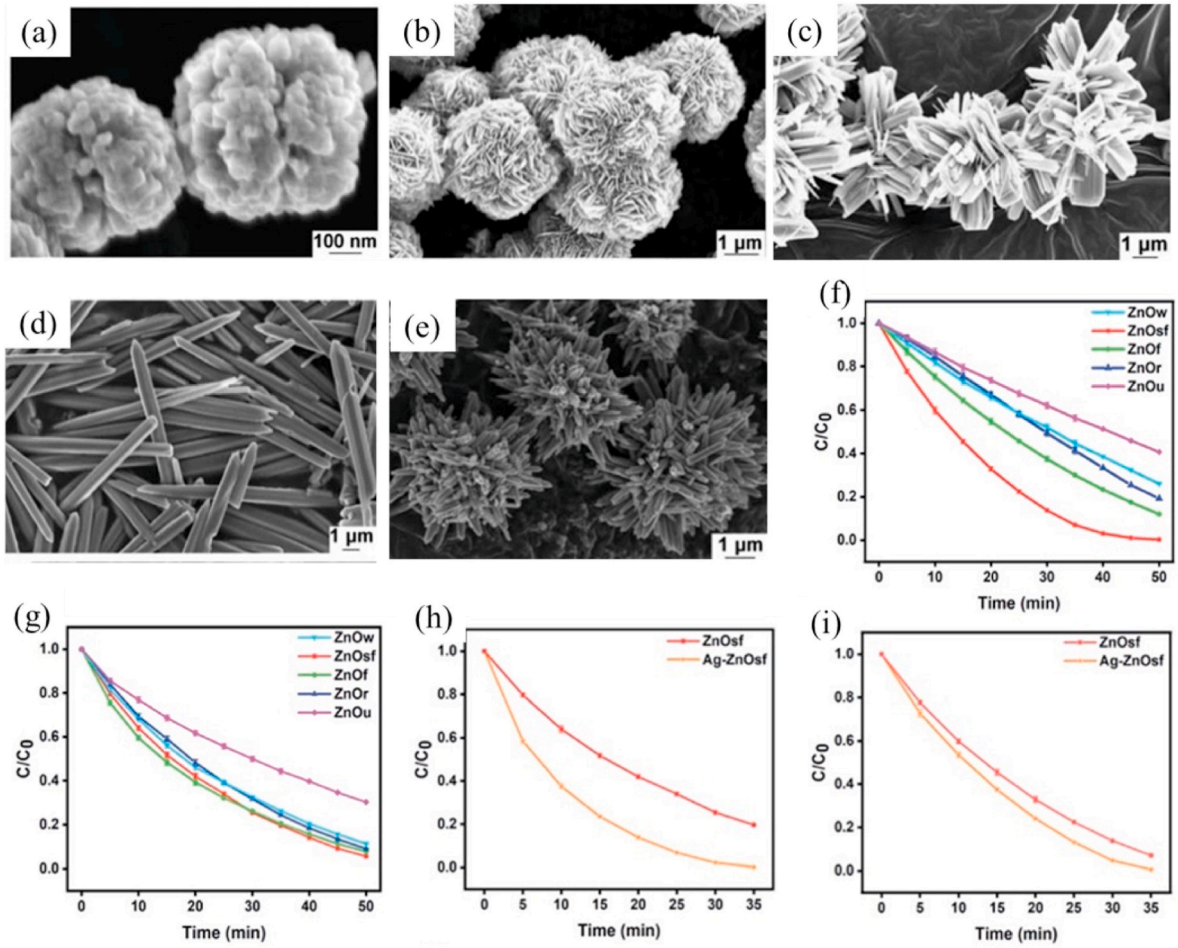

Fig. 9. SEM images of various ZnO structures (a) walnut, (b) spherical flower, (c) flower, (d) rod, and (e) urchin. The degradation rate by time of various ZnO structure for (f) MO and (g) RhB. The degradation rate comparison between Ag-ZnOsf and ZnOsf for degradation of (h) MO and (i) RhB (Lim et al., 2021).

3. Perspective

The preferred commercial adsorbent wastewater treatment at the industrial scale is activated carbon but difficult to regenerate, or produce significant toxic waste as a side-product. Composite catalytic adsorption systems could be an attractive option for dye degradation. Several researchers addressed the development of dye degradation process through adsorption, electrocoagulation process (López-Guzmán et al., 2021). The organic molecules with definite hydrophobic cavities were reported to be potential toward highly selective removal of key pollutants. The turning of calixarenes to covalent organic frameworks, or covalent organic frameworks (COFs) could be efficient due to their strong covalent bonds (Abubakar et al., 2021) shown in Fig. 10a. The metal organic framework (MOFs) is promising materials for selectively removing dyes from water. Polymerized MOF with polydopamine (PDA) would be efficient for quickly and selectively removal of high amounts of dyes and metals from water samples (Sun et al., 2018) as shown in Fig. 10b. The high stability of polyamide nanofiltration (NF) is significant for the use in acidic environment. The amide linkage of the polyamide membranes may break up under acidic conditions due to the hydrolysis of polyamide. Recently, Cao et al. (2021) reported the acid resistant membrane which may be promising for the use in acidic environment. Importantly, the stable sulfonamide structure of 3-aminobenzenesulfonamide (ABSA) could prevent the direct attack of acid, as shown in Fig. 10c. The results of laboratory-scale electrocoagulation (EC) of dyes showed promising technology elimination of particular contaminants, as reported by several researchers (Jing et al., 2021). Integration of electrocoagulation with current technology should be focused for future research. The factors including cell-design, scale-up process should be taken under consideration to make the electrocoagulation process effective. The appropriately functionalized electrodes on both the positive and negative sides could be highly efficient for selectively removal of both positive and negative toxic ions (Su et al., 2017), shown in Fig. 10d. The durability of the functionalized electrodes should be tested under real-world conditions to check the validity of the process. The development of plasma technology for the removal of contaminates from waste water could be interesting due to its low operating cost. Low pressure plasma technology should be explored for the treatment of contaminated water. The economical aspect and minimization of harmful impact should be considered for the development of any adsorbent for dye removal.

4. Conclusions

Adsorbent for dye degradation could be important tools for waste water treatment. Notably, creating anporpus structure with increased molecular interaction is important for efficient dye degradation. A high electrostatic and hydrophobic interaction is significant for the adsorption of contaminants. In particular, graphene oxide (GO) showed promising in waste water treatment but the recovery process is complex and time consuming. Adsorbent with ultrasound may be promising to reduce contaminants from waste water. Macrocopicnanosheets of aerogels showed promising for waste water treatment but simple recovering and reusing systems should be developed. Covalent organic frameworks (COFs) hols promise for selective removal of dye molecules due to its hydrophobic surface, anionic functional groups. COFs with

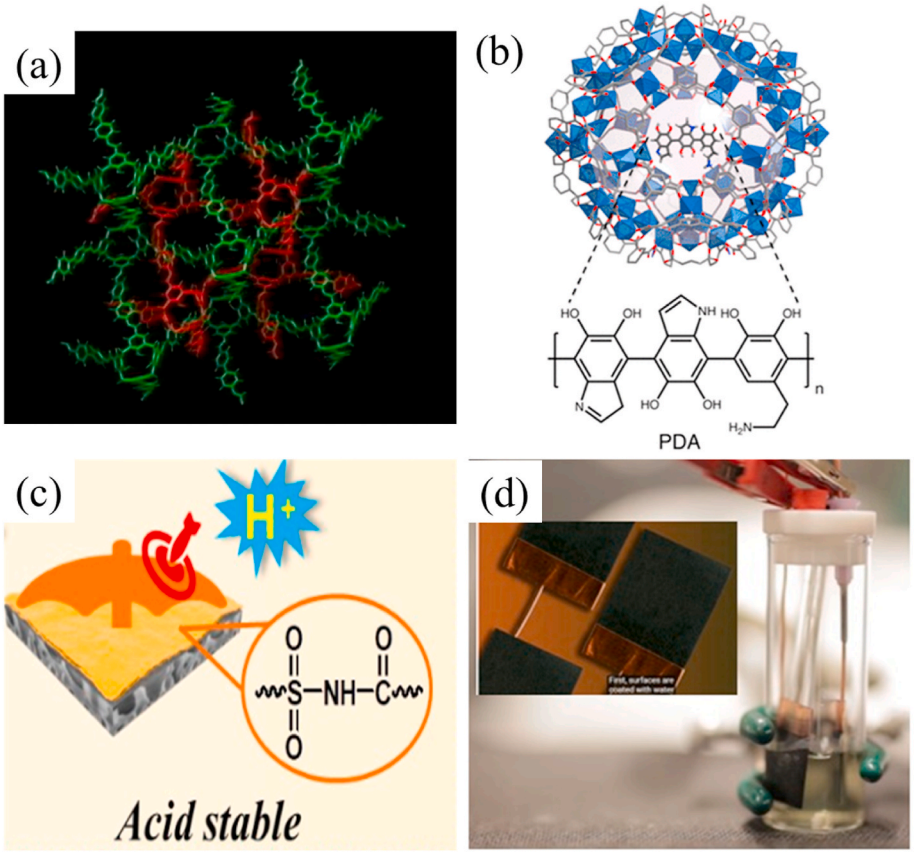

Fig. 10. Potential process for the degradation of dyes (Abubakar et al., 2021; Cao et al., 2021; Su et al., 2017; Sun et al., 2018).

controllable function could be versatile for different types of dye adsorption. Aerogel with biopolymer was found to be highly efficient towards the removal of dyes from waste water. Removal of dyes without releasing any toxic chemical is the major challenge. The removal of waste with using critical CO_2 is promising but it is still in the laboratory stage. Dye removal with electrocoagulation has been found to be effective. Integration of current technology with electrocoagulation process should be focus for the development of effective process. Any single process reported in the literature is not efficient or even suitable for the removal of all kind of dyes. An ideal adsorbent should be developed that will remove dyes efficiently without releasing any hazardous chemicals to the environment.

Declaration of competing interest

The authors declare that they have no known competing financial interests or personal relationships that could have appeared to influence the work reported in this paper.

Acknowledgements

This research was supported by the Research Management Centre of Universiti Malaysia Sabah (Grant No. SPB0005-2020) and is gratefully acknowledged. The author also wishes to thanks to the anonymous reviewers and editor for their helpful suggestions and enlightening comments.

References

Masoumi, et al., 2017. Effective synthesis of biodiesel from Jatropha curcas oil using betaine assisted nanoparticle heterogeneous catalyst from eggshell of Gallus domesticus. Renew. Energy 111, 892–905.
Sinar Mashuri, et al., 2020. Photocatalysis for organic wastewater treatment: from the basis to current challenges for society. Catalyst 10, 1260.
Abbas, K., et al., 2018. A ligand anchored conjugate adsorbent for effective mercury(II) detection and removal from aqueous media. Chem. Eng. J. 334, 432–443.
Abdulkareem-Alsultan, et al., 2022. In-situ operando and ex-situ study on light hydrocarbon-like-diesel and catalyst deactivation kinetic and mechanism study during deoxygenation of sludge oil. Chem. Eng. J. 429, 132206.
Abubakar, S., et al., 2021. Porous polycalix[n]arenes as environmental pollutant removers. ACS Appl. Mater. Interfaces 13, 14802–14815.
Ahmad, A., Azam, T., 2019. In: Grumezescu, A.M., Holban, P.W. (Eds.), 4 - Water Purification Technologies. Woodhead Publishing, pp. 83–120.
Ahmad, M.A., et al., 2014. Adsorptive removal of malachite green dye using durian seed-based activated carbon. Water Air Soil Pollut. 225, 2057.
Ahmed, F., et al., 2014. Morphological evolution of ZnO nanostructures and their aspect ratio-induced enhancement in photocatalytic properties. RSC Adv. 4, 29249–29263.
Akter, M., et al., 2021. Cellulose-based hydrogels for wastewater treatment: a concise review. Gels 7, 30.
Alam, M.M., et al., 2019. Detection of uric acid based on doped $ZnO/Ag_2O/Co_3O_4$ nanoparticle loaded glassy carbon electrode. New J. Chem. 43, 8651–8659.
Altintig, E., et al., 2017. Effective removal of methylene blue from aqueous solutions using magnetic loaded activated carbon as novel adsorbent. Chem. Eng. Res. Des. 122, 151–163.
Altintig, E., et al., 2018. Preparation, characterization and evaluation of bio-based magnetic activated carbon for effective adsorption of malachite green from aqueous solution. Mater. Chem. Phys. 220, 313–321.
Altintig, E., et al., 2021. Facile synthesis of zinc oxide nanoparticles loaded activated carbon as an eco-friendly adsorbent for ultra-removal of malachite green from water. Environ. Technol. Innovat. 21, 101305.
Angove, M.J., et al., 2019. A review on nickel(II) adsorption in single and binary component systems and future path. J. Environ. Chem. Eng. 7, 103305.
Arabkhani, P., Asfaram, A., 2020. Development of a novel three-dimensional magnetic polymer aerogel as an efficient adsorbent for malachite green removal. J. Hazard Mater. 384, 121394.
Asfaha, Y., et al., 2021. Hybrid process of electrocoagulation and electrooxidation system for wastewater treatment: a review. Clean. Eng. Technol. 4, 100261.
Asikin-Mijan, et al., 2021. A short review on catalyst, feedstock, modernised process, current state and challenges on biodiesel production. Catalyst 11, 1261.
Awual, M.R., 2015. A novel facial composite adsorbent for enhanced copper(II) detection and removal from wastewater. Chem. Eng. J. 266, 368–375.
Awual, M.R., 2016. Assessing of lead(II) capturing from contaminated wastewater using ligand doped conjugate adsorbent. Chem. Eng. J. 289, 65–73.

Awual, M.R., 2016a. Ring size dependent crown ether based mesoporous adsorbent for high cesium adsorption from wastewater. Chem. Eng. J. 303, 539–546.
Awual, M.R., 2016b. Solid phase sensitive palladium(II) ions detection and recovery using ligand based efficient conjugate nanomaterials. Chem. Eng. J. 300, 264–272.
Awual, M.R., 2017. New type mesoporous conjugate material for selective optical copper (II) ions monitoring & removal from polluted waters. Chem. Eng. J. 307, 85–94.
Awual, M.R., 2017a. Novel nanocomposite materials for efficient and selective mercury ions capturing from wastewater. Chem. Eng. J. 307, 456–465.
Awual, M.R., 2019. Innovative composite material for efficient and highly selective Pb (II) ion capturing from wastewater. J. Mol. Liq. 284, 502–510.
Awual, M.R., 2019a. Novel conjugated hybrid material for efficient lead(II) capturing from contaminated wastewater. Mater. Sci. Eng. C 101, 686–695.
Awual, M.R., 2019b. An efficient composite material for selective lead(II) monitoring and removal from wastewater. J. Environ. Chem. Eng. 7, 103087.
Awual, M.R., 2019c. Efficient phosphate removal from water for controlling eutrophication using novel composite adsorbent. J. Clean. Prod. 228, 1311–1319.
Awual, M.R., 2019d. Novel ligand functionalized composite material for efficient copper (II) capturing from wastewater sample. Compos. B Eng. 172, 387–396.
Awual, M.R., 2019e. Mesoporous composite material for efficient lead(II) detection and removal from aqueous media. J. Environ. Chem. Eng. 7, 103124.
Awual, M.R., 2019f. A facile composite material for enhanced cadmium(II) ion capturing from wastewater. J. Environ. Chem. Eng. 7, 103378.
Bakar, et al., 2013. A novel catalytic method for the synthesis of spherical aragonite nanoparticles from cockle shells. Powder Technol. 246, 434–440.
Barton, S.S., et al., 1984. Water and cyclohexane vapour adsorption on oxidized porous carbon. Carbon 22, 265–272.
Bello, K., et al., 2018. A study on adsorption behavior of newly synthesized banana pseudo-stem derived superabsorbent hydrogels for cationic and anionic dye removal from effluents. Carbohydr. Polym. 181, 605–615.
Bhagavathi Pushpa, T., et al., 2015. Investigation on removal of malachite green using EM based compost as adsorbent. Ecotoxicol. Environ. Saf. 118, 177–182.
Bhol, P., et al., 2021. Graphene-based membranes for water and wastewater treatment: a review. ACS Appl. Nano Mater. 4, 3274–3293.
Bober, P., et al., 2020. Conducting polymer composite aerogel with magnetic properties for organic dye removal. Synth. Met. 260, 116266.
Cai, C., et al., 2020a. Efficient degradation of bisphenol A in water by heterogeneous activation of peroxymonosulfate using highly active cobalt ferrite nanoparticles. J. Hazard Mater. 399, 122979.
Cai, Z., et al., 2020b. Core-shell granular activated carbon and its adsorption of trypan blue. J. Clean. Prod. 242, 118496.
Cao, Y., et al., 2021. Highly permeable acid-resistant nanofiltration membrane based on a novel sulfonamide aqueous monomer for efficient acidic wastewater treatment. Chem. Eng. J. 425, 131791.
Carvallho, M.N., et al., 2016. Dye removal from textile industrial effluents by adsorption on exfoliated graphite nanoplatelets: kinetic and equilibrium studies. Water Sci. Technol. 73, 2189–2198.
Chai, W.S., et al., 2021. A review on conventional and novel materials towards heavy metal adsorption in wastewater treatment application. J. Clean. Prod. 296, 126589.
Chan, et al., 2012. Synthesis and characterization of millimetric gamma alumina spherical particles by oil drop granulation method. J. Porous Mater. 19 (5), 807–817.
Chen, T., et al., 2018. Natural polymer konjac glucomannan mediated assembly of graphene oxide as versatile sponges for water pollution control. Carbohydr. Polym. 202, 425–433.
Chen, J., et al., 2020. Enhanced degradation of dyes by Cu-Co-Ni nanoparticles loaded on amino-modified octahedral metal–organic framework. J. Alloys Compd. 834, 155106.
Cheng, S., et al., 2019. Simultaneous removal of phosphates and dyes by Al-doped iron oxide decorated MgAl layered double hydroxide nanoflakes. Environ. Sci.: Nano 6, 2615–2625.
Cherukupally, P., et al., 2020. Surface-engineered sponges for recovery of crude oil microdroplets from wastewater. Nat. Sustain. 3, 136–143.
Choong, et al., 2019. Efficient biodiesel production from Jatropha curcus using CaSO4/Fe2O3-SiO2 core-shell magnetic nanoparticles. J. Clean. Prod. 208, 816–826.
Chowdhury, et al., 2021. Efficient cesium encapsulation from contaminated water by cellulosic biomass based activated wood charcoal. Chemosphere 262, 127801.
Chu, et al., 2013. Studies on design of heterogeneous catalysts for biodiesel production. Process Saf. Environ. Protect. 91, 131–144.
Dong, Y.D., et al., 2021. Cellulose/carbon composites and their applications in water treatment – A review. Chem. Eng. J. 405, 126980.
Duan, C., et al., 2020a. Facile synthesis of Ag NPs@ MIL-100(Fe)/guar gum hybrid hydrogel as a versatile photocatalyst for wastewater remediation: photocatalytic degradation, water/oil separation and bacterial inactivation. Carbohydr. Polym. 230, 115642.
Duan, C., et al., 2020b. Removal of heavy metals from aqueous solution using carbon-based adsorbents: a review. J. Water Process Eng. 37, 101339.
Dutta, S., et al., 2021. Recent advances on the removal of dyes from wastewater using various adsorbents: a critical review. Mater. Adv. 2, 4497–4531.
El-Katori, E.E., et al., 2020. Impact of CdS/SnO2 heterostructured nanoparticle as visible light active photocatalyst for the removal methylene blue dye. J. Photochem. Photobiol., A A392, 112403.
El-Yazeed, W.S.A., Ahmed, A.I., 2019. Photocatalytic activity of mesoporous WO3/TiO 2 nanocomposites for the photodegradation of methylene blue. Inorg. Chem. Commun. 105, 102–111.
Erickson, K., et al., 2010. Determination of the local chemical structure of graphene oxide and reduced graphene oxide. Adv. Mater. 22, 4467–4472.
Fatimah, I., et al., 2020. One-pot biosynthesis of SnO2 quantum dots mediated by Clitoria ternatea flower extract for photocatalytic degradation of rhodamine B. J. Environ. Chem. Eng. 8, 103879.
Feng, C., et al., 2020. Facile synthesis of trimethylammonium grafted cellulose foams with high capacity for selective adsorption of anionic dyes from water. Carbohydr. Polym. 241, 116369.
Fujishima, A., Zhang, X., 2006. Titanium dioxide photocatalysis: present situation and future approaches. C.R. Chim. 9, 750–760.
Gao, M., et al., 2019. Novel magnetic graphene oxide decorated with persimmon tannins for efficient adsorption of malachite green from aqueous solutions. Colloids Surf., A 566, 48–57.
Ghosh, et al., 2018. Recent progress in Si hetero-junction solar cell: a comprehensive review. Renew. Sustain. Energy Rev. 82, 1990–2004.
Gong, J.L., et al., 2009. Removal of cationic dyes from aqueous solution using magnetic multi-wall carbon nanotube nanocomposite as adsorbent. J. Hazard Mater. 164, 1517–1522.
Grbić, B., et al., 2014. TiO2/WO3 photocatalytic composite coatings prepared by spray pyrolysis. Surf. Coating. Technol. 258, 763–771.
Gu, J., et al., 2018. Reagentless preparation of shape memory cellulose nanofibril aerogels decorated with Pd nanoparticles and their application in dye discoloration. Appl. Catal., B 237, 482–490.
Guediri, A., Bouguettoucha, A., Chebli, D., Chafai, N., Amrane, A., 2020. Molecular dynamic simulation and DFT computational studies on the adsorption performances of methylene blue in aqueous solutions by orange peel-modified phosphoric acid. J. Mol. Struct. 1202, 127290.
Gupta, K., Khatri, O.P., 2017. Reduced graphene oxide as an effective adsorbent for removal of malachite green dye: plausible adsorption pathways. J. Colloid Interface Sci. 501, 11–21.
Haafiz, et al., 2017. Evaluation of mechanical, morphological, and biodegradable properties of hybrid natural fiber polymer nanocomposites. Polym. Compos. 38 (3), 583–587.
Hameed, A.M., 2020. Synthesis of Si/Cu amorphous adsorbent for efficient removal of methylene blue dye from aqueous media. J. Inorg. Organomet. Polym. Mater. 30, 2881–2889.
Han, J., et al., 2018. Mesoporous TiO2 with WO3 functioning as dopant and light-sensitizer: a highly efficient photocatalyst for degradation of organic compound. J. Hazard Mater. 358, 44–52.
Han, D., et al., 2021. A review of studies using hydrocarbon adsorption material for reducing hydrocarbon emissions from cold start of gasoline engine. Renew. Sustain. Energy Rev. 135, 110079.
Hasan, M.M., 2015. Fine-tuning mesoporous adsorbent for simultaneous ultra-trace palladium(II) detection, separation and recovery. J. Ind. Eng. Chem. 21, 507–515.
Hasan, M.M., 2019. A ligand based innovative composite material for selective lead(II) capturing from wastewater. J. Mol. Liq. 294, 111679.
Hasan, M.M., et al., 2015. Organic-inorganic based nano-conjugate adsorbent for selective palladium(II) detection, separation and recovery. Chem. Eng. J. 259, 611–619.
Hasan, M.M., et al., 2021. Sustainable composite sensor material for optical cadmium(II) monitoring and capturing from wastewater. Microchem. J. 161, 105800.
Hasan, M.N., et al., 2021a. Optical detection and recovery of Yb(III) from waste sample using novel sensor ensemble nanomaterials. Microchem. J. 162, 105868.
Hayase, et al., 2021. Recent advancements and opportunities of decorated graphitic carbon nitride towards solar fuel production and beyond. Sustain. Energy Fuels 5, 4457–4511.
He, S., et al., 2018. High efficient visible-light photocatalytic performance of Cu/ZnO/rGO nanocomposite for decomposing of aqueous ammonia and treatment of domestic wastewater. Front. Chem. 6, 219.
Hena, S., et al., 2018. Synthesis a novel multilamellar mesoporous TiO2/ZSM-5 for photo-catalytic degradation of methyl orange dye in aqueous media. J. Environ. Chem. Eng. 6, 218–227.
Hessou, E.P., et al., 2019. A first principle evaluation of the adsorption mechanism and stability of volatile organic compounds into NaY zeolite. Z. für Kristallogr. - Cryst. Mater. 234, 469–482.
Hong, Y., et al., 2020. Nitrogen-rich magnetic bio-activated carbon from sericin: a fast removable and easily separable superadsorbent for anionic dye removal. Macromol. Res. 28, 986–996.
How, et al., 2017. Extraction and characterization of γ-alumina from waste aluminium dross. Waste Biomass Valorization 8, 321–327.
Hu, X.S., et al., 2018. Super-adsorbent hydrogel for removal of methylene blue dye from aqueous solution. J. Mater. Chem. A 6, 17612–17624.
Huang, Y., et al., 2012. Preparation and swelling properties of graphene oxide/poly (acrylic acid-co-acrylamide) super-absorbent hydrogel nanocomposites. Colloids Surf A401, 97–106.
Hussain, M.M., et al., 2019. Arsenic sensor development based on modification with (E)-N′-(2-nitrobenzylidine)- benzenesulfonohydrazide: a real sample analysis. New J. Chem. 43, 9066–9075.
Ibrahim, et al., 2021a. Novel micro-structured carbon-based adsorbents for notorious arsenic removal from wastewater. Chemosphere 272, 129653.
Ibrahim, et al., 2021b. Step towards the sustainable toxic dyes removal and recycling from aqueous solution-A comprehensive review. Resour. Conserv. Recycl. 175, 105849.
Igwegbe, C., et al., 2021. Electrocoagulation-flocculation of aquaculture effluent using hybrid iron and aluminium electrodes: a comparative study. Chem. Eng. J. 6, 100107.

Ikram, M., et al., 2020. 2D chemically exfoliated hexagonal boron nitride (hBN) nanosheets doped with Ni: synthesis, properties and catalytic application for the treatment of industrial wastewater. Appl. Nanosci. 10, 3525–3528.
Ikram, M., et al., 2020a. Photocatalytic and bactericidal properties and molecular docking analysis of TiO2nanoparticles conjugated with Zr for environmental remediation. RSC Adv. 10, 30007–30024.
Ikram, M., et al., 2020b. Dye degradation performance, bactericidal behavior and molecular docking analysis of Cu-doped TiO2nanoparticles. RSC Adv. 10, 24215–24233.
Ismail, A.A., et al., 2016. Ease synthesis of mesoporous WO3–TiO2 nanocomposites with enhanced photocatalytic performance for photodegradation of herbicide imazapyr under visible light and UV illumination. J. Hazard Mater. 307, 43–54.
Ivan-Tan, et al., 2017. Screening of solid base catalysts on palm oil based biolubricant synthesis. J. Clean. Prod. 148, 441–451.
Jamshidi, M., et al., 2016. Sonochemical assisted hydrothermal synthesis of ZnO: Cr nanoparticles loaded activated carbon for simultaneous ultrasound-assisted adsorption of ternary toxic organic dye: derivative spectrophotometric, optimization, kinetic and isotherm study. Ultrason. Sonochem. 32, 119–131.
Janaun, et al., 2016. Synthesis of structured carbon nanorods for efficient hydrogen storage. Mater. Lett. 179, 57–60.
Javaid, R., Qazi, U., 2019. Catalytic oxidation process for the degradation of synthetic dyes : an overview. Int. J. Environ. Res. Publ. Health 16, 1–27.
Jiang, F., et al., 2017. Adsorption and desorption of cationic malachite green dye on cellulose nanofibril aerogels. Carbohydr. Polym. 173, 286–294.
Jiang, W., et al., 2021. Adsorption of cationic dye from water using an iron oxide/activated carbon magnetic composites prepared from sugarcane bagasse by microwave method. Environ. Technol. 42, 337–350.
Jing, G., et al., 2021. Electrocoagulation for industrial wastewater treatment: an updated review. Environ. Sci. Water Res. Technol. 7, 1177–1196.
Kamel, R.M., et al., 2019. Efficient toxic nitrite monitoring and removal from aqueous media with ligand based conjugate materials. J. Mol. Liq. 285, 20–26.
Kasinathan, M., et al., 2020. A facile fabrication of Br-modified g-C3N4/rGO composite catalyst for enhanced visible photocatalytic activity towards the degradation of harmful dyes. Mater. Res. Bull. 130, 110870.
Kataki, S., et al., 2021. Concerns and strategies for wastewater treatment during COVID-19 pandemic to stop plausible transmission. Resour. Conserv. Recycl. 164, 105156.
Khalil, et al., 2020. Preparation of Na2O supported CNTs nanocatalyst for efficient biodiesel production from waste-oil. Energy Convers. Manag. 205, 112445.
Khan, M., Lo, I.M.C., 2016. A holistic review of hydrogel applications in the adsorptive removal of aqueous pollutants: recent progress, challenges, and perspectives. Water Res. 106, 259–271.
Khan, et al., 2021a. Improving valuable metal ions capturing from spent Li-ion batteries with novel materials and approaches. J. Mol. Liq. 338, 116703.
Khan, F.S.A., et al., 2021b. A comprehensive review on magnetic carbon nanotubes and carbon nanotube-based buckypaper for removal of heavy metals and dyes. J. Hazard Mater. 413, 125375.
Khandaker, S., et al., 2021. Functionalized layered double hydroxides composite bio-adsorbent for efficient copper(II) ion encapsulation from wastewater. J. Environ. Manag. 300, 113782.
Kobayashi, T., et al., 2020. Improving cesium removal to clean-up the contaminated water using modified conjugate material. J. Environ. Chem. Eng. 8, 103684.
Kubra, K.T., et al., 2021a. Enhanced toxic dye removal from wastewater using biodegradable polymeric natural adsorbent. J. Mol. Liq. 328, 115468.
Kubra, et al., 2021b. Utilizing an alternative composite material for effective copper(II) ion capturing from wastewater. J. Mol. Liq. 336, 116325.
Kumar, A., Kaur, H., 2020. Sprayed in-situ synthesis of polyvinyl alcohol/chitosan loaded silver nanocomposite hydrogel for improved antibacterial effects. IInt. J. Biol. Macromol. 145, 950–964.
Kusior, A., et al., 2019. Shaped Fe2O3 nanoparticles – synthesis and enhanced photocatalytic degradation towards RhB. Appl. Surf. Sci. 476, 342–352.
Lai, C.W., Sreekantan, S., 2013a. Incorporation of WO3 species into TiO2 nanotubes via wet impregnation and their water-splitting performance. Electrochim. Acta 87, 294–302.
Lai, C.W., Sreekantan, S., 2013b. Preparation of hybrid WO3–TiO2 nanotube photoelectrodes using anodization and wet impregnation: improved water-splitting hydrogen generation performance. Int. J. Hydrogen Energy 38, 2156–2166.
Lee, et al., 2019. A review on thermal conversion of plant oil (edible and inedible) into green fuel using carbon-based nanocatalyst. Catalyst 9, 350.
Lei, C., et al., 2017. Superb adsorption capacity of hierarchical calcined Ni/Mg/Al layered double hydroxides for Congo red and Cr(VI) ions. J. Hazard Mater. 321, 801–811.
Li, W.H., et al., 2011. Preparation and utilization of sludge-based activated carbon for the adsorption of dyes from aqueous solutions. Chem. Eng. J. 171, 320–327.
Li, J., et al., 2016. Magnetic polydopamine decorated with Mg–Al LDH nanoflakes as a novel bio-based adsorbent for simultaneous removal of potentially toxic metals and anionic dyes. J. Mater. Chem. A 4, 1737–1746.
Li, Y., et al., 2019. MoS2 with structure tuned photocatalytic ability for degradation of methylene blue. IOP Conf. Ser. Earth Environ. Sci. 300, 52021.
Lim, H., et al., 2021. Efficient photocatalytic degradation of dyes using photo-deposited Ag nanoparticles on ZnO structures: simple morphological control of ZnO. RSC Adv. 11, 8709–8717.
Ling, S., et al., 2021. Design and function of biomimetic multilayer water purification membranes. Sci. Adv. 3, e1601939.
Liu, F., et al., 2016. Effect of pore structure on the adsorption of aqueous dyes to ordered mesoporous carbons. Microporous Mesoporous Mater. 227, 104–111.
Liu, X., et al., 2019a. Enhanced dyes adsorption from wastewater via Fe3O4 nanoparticles functionalized activated carbon. J. Hazard Mater. 373, 397–407.
Liu, Y., et al., 2019b. Preparation of magnetic Fe3O4/MIL-88A nanocomposite and its adsorption properties for bromophenol blue dye in aqueous solution. Nanomaterials 9, 51.
López-Guzmán, M., et al., 2021. Electrocoagulation process: an approach to continuous processes, reactors design, pharmaceuticals removal, and hybrid systems - a review. Processes 9, 1831.
Lou, L., et al., 2019. Visible light photocatalytic functional TiO2/PVDF nanofibers for dye pollutant degradation. Part. Part. Syst. Char. 36, 900091.
Lu, P.J., et al., 2011. Chemical regeneration of activated carbon used for dye adsorption. J. Taiwan Inst. Chem. Eng. 42, 305–311.
Lway Faisal Abdulrazak, et al., 2021. Towards energy sustainability: Bangladesh perspectives. Energy Strat. Rev. 3, 100738.
Ma, J., et al., 2012. Enhanced adsorptive removal of methyl orange and methylene blue from aqueous solution by alkali-activated multiwalled carbon nanotubes. ACS Appl. Mater. Interfaces 4, 5749–5760.
Ma, J., et al., 2014. Mechanism of 2,4-dinitrophenol photocatalytic degradation by ζ-Bi2O3/Bi2MoO6 composites under solar and visible light irradiation. Chem. Eng. J. 251, 371–380.
Madan, S., et al., 2019. Adsorption dynamics of Congo red dye removal using ZnO functionalized high silica zeolitic particles. Appl. Surf. Sci. 487, 907–917.
Mahapatra, A., et al., 2013. Adsorptive removal of Congo red dye from wastewater by mixed iron oxide–alumina nanocomposites. Ceram. Int. 39, 5443–5451.
Makhado, E., et al., 2018. Microwave assisted synthesis of xanthan gum-cl-poly (acrylic acid) based-reduced graphene oxide hydrogel composite for adsorption of methylene blue and methyl violet from aqueous solution. Int. J. Biol. Macromol. 119, 255–269.
Malato, S., et al., 2009. Decontamination and disinfection of water by solar photocatalysis: recent overview and trends. Catal. Today 147, 1–59.
Manjari, G., et al., 2020. Facile green synthesis of Ag–Cu decorated ZnO nanocomposite for effective removal of toxic organic compounds and an efficient detection of nitrite ions. J. Environ. Manag. 262, 110282.
Mansa, et al., 2012. The effect of low air-to-liquid mass flow rate ratios on the size, size distribution and shape of calcium alginate particles produced using the atomization method. J. Food Eng. 108, 297–303.
Mansir, et al., 2019. Facile recoverable and reusable macroscopic alumina supported Ni-based catalyst for efficient hydrogen production. Sci. Rep. 9 (1), 1–14.
Marwani, H.M., et al., 2017. Trace electrochemical detection of Ni^{2+} ions with bidentate N, N'-(ethane-1,2-diyl)bis(3,4-dimethoxybenzenesulfonamide) [EDBDMBS] as a chelating agent. Inorg. Chim. Acta. 464, 157–166.
Miah, M.R., et al., 2021. Sustainable approach for wastewater treatment using microbial fuel cells and green energy generation- A comprehensive review. J. Mol. Liq. 344, 117795.
Mohammadzadeh Kakhki, R., et al., 2017. New and highly efficient Ag doped ZnO visible nano photocatalyst for removing of methylene blue. J. Mater. Sci. Mater. Electron. 28, 5941–5952.
Mondal, M.A.H., et al., 2021. A snapshot of coal-fired power generation in Bangladesh: a demand–supply outlook. Nat. Resour. Forum 45, 157–182.
Monir, M.U., et al., 2021. Energy challenges for a clean environment: Bangladesh's experience. Energy Rep. 7, 3373–3389.
Moniruzzaman, et al., 2014. Advances in solid-catalytic and non-catalytic technologies for biodiesel production. Energy Convers. Manag. 88, 1200–1218.
Moosavi, S., et al., 2020. Application of efficient magnetic particles and activated carbon for dye removal from wastewater. ACS Omega 5, 20684–20697.
Mutalib, et al., 2020. SiO 2-Rich sugar cane bagasse ash catalyst for transesterification of palm oil. Bioenergy Res 13 (3), 986–997.
Najafi, H., et al., 2021. A comprehensive study on modified-pillared clays as an adsorbent in wastewater treatment processes. Process Saf. Environ. Protect. 147, 8–36.
Naseeruteen, F., et al., 2018. Adsorption of malachite green from aqueous solution by using novel chitosan ionic liquid beads. Int. J. Biol. Macromol. 107, 1270–1277.
Nasir, A.M., et al., 2021. Recent progress on fabrication and application of electrospun nanofibrous photocatalytic membranes for wastewater treatment: a review. J. Water Process Eng. 40, 101878.
Nasrollahzadeh, M., et al., 2021. Carbon-based sustainable nanomaterials for water treatment: state-of-art and future perspectives. Chemosphere 263, 128005.
Naushad, M., et al., 2019. Adsorption of textile dye using para-aminobenzoic acid modified activated carbon: kinetic and equilibrium studies. J. Mol. Liq. 296, 112075.
Ng, C.H., et al., 2017. Capacitive performance of graphene-based asymmetric supercapacitor. Electrochim. Acta 229, 173–182.
Ng, et al., 2018. Methoxy-functionalized mesostructured stable carbon catalysts for effective biodiesel production from non-edible feedstock. Chem. Eng. J. 334, 1851–1868.
Nizam, N.U.M., et al., 2021. The removal of anionic and cationic dyes from an aqueous solution using biomass-based activated carbon. Sci. Rep. 11, 1–17.
Okafor, C.C., et al., 2021. Sustainable management of textile and clothing. Clean Technol.Recyl. 1, 70–87.
Pan, Y., et al., 2019. Novel cellulose/montmorillonite mesoporous composite beads for dye removal in single and binary systems. Bioresour. Technol. 286, 121366.
Pandey, S., et al., 2020. Fast and highly efficient catalytic degradation of dyes using κ-carrageenan stabilized silver nanoparticles nanocatalyst. Carbohydr. Polym. 230, 115597.
Park, S.Y., et al., 2015. Eco-friendly carbon-nanodot-based fluorescent paints for advanced photocatalytic systems. Sci. Rep. 5, 12420.
Pereira, A.G.B., et al., 2021. Recent advances on composite hydrogels designed for the remediation of dye-contaminated water and wastewater: a review. J. Clean. Prod. 284, 124703.

Qi, X., et al., 2021. Recent advances in polysaccharide-based adsorbents for wastewater treatment. J. Clean. Prod. 315, 128221.
Qu, J., et al., 2020. Visible-light-responsive K-doped g-C3N4/BiOBr hybrid photocatalyst with highly efficient degradation of Rhodamine B and tetracycline. Mater. Sci. Semicond. Process. 112, 105023.
Qurrat-Ul-Ain, et al., 2019. Anionic azo dyes removal from water using amine-functionalized cobalt-iron oxide nanoparticles: a comparative time-dependent study and structural optimization towards the removal mechanism. RSC Adv. 10, 1021–1041.
Rachel-Tang, et al., 2017. Bio-oil production via catalytic solvolysis of biomass. RSC Adv. 7, 7820–7830.
Rafiq, A., et al., 2021. Photocatalytic degradation of dyes using semiconductor photocatalysts to clean industrial water pollution. J. Ind. Eng. Chem. 97, 111–128.
Rahman, M.M., et al., 2018. 4-Hexylresorcinol sensor development based on wet-chemically prepared Co3O4@Er2O3 nanorods: a practical approach. J. Ind. Eng. Chem. 66, 446–455.
Rahman, et al., 2020. Current treatment technologies and mechanisms for removal of indigo carmine dyes from wastewater: a review. J. Mol. Liq. 114061.
Rathi, B.S., Kumar, P.S., 2021. Application of adsorption process for effective removal of emerging contaminants from water and wastewater. Environ. Pollut. 280, 116995.
Ray, S.K., et al., 2021. A critical review on strategies for improving efficiency of BaTiO3-based photocatalysts for wastewater treatment. J. Environ. Manag. 290, 112679.
Rodrigues, J., et al., 2020. Photocatalytic degradation using ZnO for the treatment of RB 19 and RB 21 dyes in industrial effluents and mathematical modeling of the process. Chem. Eng. Res. Des. 153, 294–305.
Roy, S., et al., 2022. Functional novel ligand based palladium(II) separation and recovery from e-waste using solvent-ligand approach. Colloids Surf., A 632, 127767.
Saeed, A., et al., 2010. Application potential of grapefruit peel as dye sorbent: kinetics, equilibrium and mechanism of crystal violet adsorption. J. Hazard Mater. 179, 564–572.
Saleh, T.A., et al., 2020. Synthesis of silica nanoparticles grafted with copolymer of acrylic acrylamide for ultra-removal of methylene blue from aquatic solutions. Eur. Polym. J. 130, 109698.
Salem, A.N.M., et al., 2016. Selective adsorption of amaranth dye on Fe3O4/MgO nanoparticles. J. Mol. Liq. 219, 780–788.
Salman, M.S., et al., 2021. Sustainable detection and capturing of cerium(III) using ligand embedded solid-state conjugate adsorbent. J. Mol. Liq. 338, 116667.
Sandoval, A., et al., 2017. Titanate nanotubes for removal of methylene blue dye by combined adsorption and photocatalysis. Fuel 198, 22–30.
Santhi, T., et al., 2016. A new alternative adsorbent for the removal of cationic dyes from aqueous solution. Arab. J. Chem. 9, S466–S474.
Shahat, A., et al., 2021. Novel solid-state sensor material for efficient cadmium(II) detection and capturing from wastewater. Microchem. J. 164, 105967.
Sheikh, M.S., et al., 2016. Treatment of copper(II) containing wastewater by a newly developed ligand based facial conjugate materials. Chem. Eng. J. 288, 368–376.
Shenashen, M.A., et al., 2020. Biodegradable natural carbohydrate polymeric sustainable adsorbents for efficient toxic dye removal from wastewater. J. Mol. Liq. 319, 114356.
Shenashen, M.A., et al., 2021. Assessing of cesium removal from wastewater using functionalized wood cellulosic adsorbent. Chemosphere 270, 128668.
Shenashen, M.A., et al., 2021a. Natural biodegradable polymeric bioadsorbents for efficient cationic dye encapsulation from wastewater. J. Mol. Liq. 323, 114587.
Shende, R.V., Mahajani, V.V., 2002. Wet oxidative regeneration of activated carbon loaded with reactive dye. Waste Manag. 22, 73–83.
Sheth, Y., et al., 2021. An environment friendly approach for heavy metal removal from industrial wastewater using chitosan based biosorbent: a review. Sustain.Energy Technol. Assess. 43, 100951.
Singh, A., et al., 2021. Synthesis of Ag nanoparticle supported graphene/multi-walled carbon nanotube based nanohybrids for photodegradation of toxic dyes. Mater. Express 11, 936–946.
Siong, V.L.E., et al., 2019. Removal of methylene blue dye by solvothermally reduced graphene oxide: a metal-free adsorption and photodegradation method. RSC Adv. 9, 37686–37695.
Solangi, N.H., et al., 2021. Development of fruit waste derived bio-adsorbents for wastewater treatment: a review. J. Hazard Mater. 416, 125848.
Sridharan, K., et al., 2013. Novel visible light active graphitic C3N4–TiO2 composite photocatalyst: synergistic synthesis, growth and photocatalytic treatment of hazardous pollutants. Appl. Catal., B 142–143, 718–728.
Stojadinović, S., et al., 2012. Photocatalytic properties of TiO2/WO3 coatings formed by plasma electrolytic oxidation of titanium in 12-tungstosilicic acid. Appl. Catal., B 126, 334–341.
Su, X., et al., 2017. Asymmetric Faradaic systems for selective electrochemical separations. Energy Environ. Sci. 10, 1272–1283.
Sultana, et al., 2020. Advances in sustainable approaches to recover metals from e-waste-A review. J. Clean. Prod. 244, 118815.
Sun, D., et al., 2018. Rapid, selective heavy metal removal from water by a metal–organic framework/polydopamine composite. ACS Cent. Sci. 4, 349–356.
Sunaina, et al., 2020. Mechanistic insights of enhanced photocatalytic efficiency of SnO2-SnS2 heterostructures derived from partial sulphurization of SnO2. Separ. Purif. Technol. 242, 116835.
Suresh, R., et al., 2021. Recent advancements of spinel ferrite based binary nanocomposite photocatalysts in wastewater treatment. Chemosphere 274, 129734.
Suzuki, S., et al., 2014. Radioactive cesium removal from nuclear wastewater by novel inorganic and conjugate adsorbents. Chem. Eng. J. 242, 127–135.
Suzuki, S., et al., 2015. Ultimate selenium(IV) monitoring and removal from water using a new class of organic ligand based composite adsorbent. J. Hazard Mater. 291, 111–119.
Swaraz, et al., 2021. Advances in physiochemical and biotechnological approaches for sustainable metal recovery from e-waste: a critical review. J. Clean. Prod. 323, 129015.
Syazwani, et al., 2017. Transesterification activity and characterization of natural CaO derived from waste venus clam (Tapes belcheri S.) material for enhancement of biodiesel production. Process Saf. Environ. Protect. 105, 303–315.
Taguchi, T., et al., 2014. Selective cesium removal from radioactive liquid waste by crown ether immobilized new class conjugate adsorbent. J. Hazard Mater. 278, 227–235.
Taguchi, T., et al., 2016. Encapsulation of cesium from contaminated water with highly selective facial organic-inorganic mesoporous hybrid adsorbent. Chem. Eng. J. 291, 128–137.
Taufiq-Yap, Y.H., et al., 2019. Improving the hydrogen production from water over MgO promoted Ni-Si/CNTs photocatalyst. J. Clean. Prod. 238, 117887.
Taufiq-Yap, Y.H., et al., 2021. Towards the robust hydrogen (H2) fuel production with niobium complexes-A review. J. Clean. Prod. 318, 128439.
Teo, S.H., et al., 2021. Introducing the novel composite photocatalysts to boost the performance of hydrogen (H_2) production. J. Clean. Prod. 313, 127909.
Thommes, M., et al., 2015. Physisorption of gases, with special reference to the evaluation of surface area and pore size distribution (IUPAC Technical Report). Pure Appl. Chem. 87, 1051–1069.
Toyohara, Y., et al., 2020. Development of synthetic zeolites from bio-slag for cesium adsorption: kinetic, isotherm and thermodynamic studies. J. Water Process Eng. 33, 101055.
Tuzen, M., et al., 2018. Response surface optimization, kinetic and thermodynamic studies for effective removal of rhodamine B by magnetic AC/CeO2 nanocomposite. J. Environ. Manag. 206, 170–177.
Uddin, M.J., et al., 2021. Adsorptive removal of dyes from wastewater using a metal-organic framework: a review. Chemosphere 284, 131314.
UNICEF, 2019. 1 in 3 People Globally Do Not Have Access to Safe Drinking Water – UNICEF, WHO [WWW Document]. New York, Geneva. URL. https://www.who.int/news/item/18-06-2019-1-in-3-people-globally-do-not-have-access-to-safe-drinking-water-unicef-who, 10.20.21.
Velusamy, S., et al., 2021. A review on heavy metal ions and containing dyes removal through graphene oxide-based adsorption strategies for textile wastewater treatment. Chem. Rec. 21, 1570–1610.
Wang, J.L., et al., 2012. Advanced oxidation processes for wastewater treatment: formation of hydroxyl radical and application. Crit. Rev. Environ. Sci. Technol. 42, 251–325.
Wang, X., et al., 2019. Effect of pyrolysis temperature on characteristics, chemical speciation and risk evaluation of heavy metals in biochar derived from textile dyeing sludge. Ecotoxicol. Environ. Saf. 168, 45–52.
Wang, K., et al., 2021. Flocculation-to-adsorption transition of novel salt-responsive polyelectrolyte for recycling of highly polluted saline textile effluents. Chem. Eng. J. 413, 127410.
Wong, S., et al., 2020. Effective removal of anionic textile dyes using adsorbent synthesized from coffee waste. Sci. Rep. 10, 2928.
Xia, M., et al., 2019. Removal of Hg(ii) in aqueous solutions through physical and chemical adsorption principles. RSC Adv. 9, 20941–20953.
Xiao, J., et al., 2020. Highly selective removal of cationic dyes from water by acid-base regulated anionic functionalized polyacrylonitrile fiber: fast adsorption, low detection limit. Reusability. React. Funct. Polym. 146, 104394.
Yadav, S., et al., 2020. Cationic dye removal using novel magnetic/activated charcoal/β-cyclodextrin/alginate polymer nanocomposite. Nanomaterials 10, 170.
Yaita, T., et al., 2013. Design a novel optical adsorbent for simultaneous ultra-trace cerium(III) detection, sorption and recovery. Chem. Eng. J. 228, 327–335.
Yaita, T., et al., 2015. A sensitive ligand embedded nano-conjugate adsorbent for effective cobalt(II) ions capturing from contaminated water. Chem. Eng. J. 276, 1–10.
Yang, X., et al., 2019. Synthesis and photocatalytic property of cubic phase CdS. Solid State Sci. 92, 31–35.
Yao, Y., et al., 2012. Synthesis, characterization, and adsorption properties of magnetic Fe3O4@graphene nanocomposite. Chem. Eng. J. 84, 326–332.
Yin, W., et al., 2017. Solvothermal synthesis of magnetic CoFe2O4/rGO nanocomposites for highly efficient dye removal in wastewater. RSC Adv. 7, 4062–4069.
Yin, J., et al., 2020. Precipitated droplets in-situ cross-linking polymerization towards hydrogel beads for ultrahigh removal of positively charged toxins. Separ. Purif. Technol. 238, 116497.
Yu, B., et al., 2016. Photocatalytic reduction of CO2 over Ag/TiO2 nanocomposites prepared with a simple and rapid silver mirror method. Nanoscale 8, 11870–11874.
Yu, S., et al., 2021. Recent advances in metal-organic framework membranes for water treatment: a review. Sci. Total Environ. 800, 149662.
Zafar, et al., 2019. Effective adsorptive removal of azo dyes over spherical ZnO nanoparticles. J. Mater. Res. Technol. 8, 713–725.
Zainal, et al., 2019. Pyro-lytic de-oxygenation of waste cooking oil for green diesel production over Ag2O3-La2O3/AC nano-catalyst. J. Anal. Appl. Pyrolysis 137, 171–184.
Zayed, M., et al., 2019. Synthesis and characterization of nanoporous ZnO and Pt/ZnO thin films for dye degradation and water splitting applications. Int. J. Hydrogen Energy 17630–17648.
Zhan, S., et al., 2017. Efficient NH3-SCR removal of NOx with highly ordered mesoporous WO3(χ)-CeO2 at low temperatures. Appl. Catal., B 203, 199–209.

Zhang, Z., Kong, J., 2011. Novel magnetic Fe3O4@C nanoparticles as adsorbents for removal of organic dyes from aqueous solution. J. Hazard Mater. 193, 325–329.
Zhang, J., et al., 2008. Importance of the relationship between surface phases and photocatalytic activity of TiO2. Angew. Chem. Int. Ed. 47, 1766–1769.
Zhang, H., et al., 2016. Laser induced fabrication of mono-dispersed Ag2S@Ag nanoparticles and their superior adsorption performance for dye removal. Opt. Mater. Express 6, 2573–2583.
Zhang, F., et al., 2017. Effective adsorption of malachite green using magnetic barium phosphate composite from aqueous solution. Spectrochim. Acta, Part A 182, 116–122.
Zhang, X., et al., 2018. Preparation of novel oxidized mesoporous carbon with excellent adsorption performance for removal of malachite green and lead ion. Appl. Surf. Sci. 442, 322–331.
Zhang, R., et al., 2020a. Photocatalytic Poly(vinylidene fluoride) membrane of Ag3PO4/GO/APTES for water treatment. Colloids Surf A597, 124779.
Zhang, W., et al., 2020b. Robust shape-retaining nanocellulose-based aerogels decorated with silver nanoparticles for fast continuous catalytic discoloration of organic dyes. Separ. Purif. Technol. 242, 116523.
Zhao, J., et al., 2020. Novel Z-scheme heterogeneous photo-Fenton-like g-C3N4/FeOCl for the pollutants degradation under visible light irradiation. J. Photochem. Photobiol., A A391, 112343.
Zheng, K., et al., 2019. Controllable synthesis of honeycomb-structured ZnO nanomaterials for photocatalytic degradation of methylene blue. Mater. Lett. 253, 30–33.
Zhou, L., et al., 2019. Simultaneous removal of mixed contaminants, copper and norfloxacin, from aqueous solution by ZIF-8. Chem. Eng. J. 362, 628–637.
Zhu, Y., et al., 2019. Removal of chelated heavy metals from aqueous solution: a review of current methods and mechanisms. Sci. Total Environ. 678, 253–266.
Zirak, M., et al., 2018. Carboxymethyl cellulose coated Fe3O4@SiO2 core–shell magnetic nanoparticles for methylene blue removal: equilibrium, kinetic, and thermodynamic studies. Cellulose 25, 503–515.
Znad, H., et al., 2021. Efficient encapsulation of toxic dye from wastewater using biodegradable polymeric adsorbent. J. Mol. Liq. 329, 115541.
Znad, H., et al., 2021a. Optimization of innovative composite sensor for Pb(II) detection and capturing from water samples. Microchem. J. 160, 105765.